ACS Catalysis

Review

pubs.acs.org/acscatalysis

Computational Mechanistic Studies on Reactions of Transition Metal Complexes with Noninnocent Pincer Ligands: Aromatization–Dearomatization or Not

Haixia Li* and Michael B. Hall

Department of Chemistry, Texas A&M University, College Station, Texas 77843-3255, United States

ABSTRACT: The development of green chemistry has attracted chemists' attentions in recent years. Among them, Milstein and co-workers have discovered a new mode of metal–ligand cooperation in complexes in which an aromatization–dearomatization process of the pyridine- or acridine-based PNP and PNN "pincer" ligands appears to be a key element. These complexes were reported to lead to unusual X–H (X = H, C, O, N, and B) activation reactions and to environmentally benign catalysis involving dehydrogenative coupling reactions and hydrogenation reactions, representing an important development in green chemistry. This review provides a summary of theoretical studies on the mechanisms of the reactions mediated by transition metal complexes with noninnocent pincer ligands synthesized by Milstein and co-workers. The aromatization–dearomatization process of the pyridine- or acridine-based PNP and PNN "pincer" ligands were found to play important roles in some reactions, while other reactions do not involve the aromatization–dearomatization process. For some reactions, several research groups proposed different mechanisms to explain the same reaction. Thus, to compare these mechanisms, we recalculate their rate-determining steps by using the functionals that are calibrated to produce results close to those from coupled cluster calculations. Moreover, the understanding of the reaction mechanisms can help researchers to improve the current reactions and design new reactions.

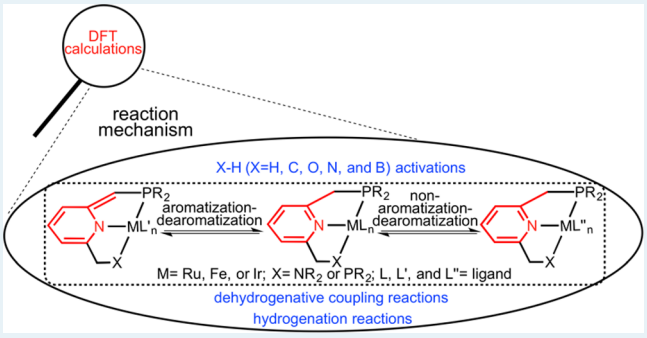

KEYWORDS: *DFT calculations, mechanistic studies, transition-metal complexes with noninnocent pincer ligands, pyridine-based ligands, acridine-based ligands, aromatization–dearomatization, catalysis, σ-bond activation, dehydrogenative coupling reactions, hydrogenation reactions*

1. INTRODUCTION

Because of the resource depletion and environmental concerns, chemists and chemical industries have been working to discover environmentally benign synthetic methods and sustainable catalytic reactions that avoid toxic reagents and waste productions. Reactions mediated by the transition metal complexes have been applied widely both in synthesis and in catalysis. Most of these reactions are based on the metal center, and their surrounding ligands are innocent,[1] a term used for ligands that support the properties of the metal centers but do not participate in breaking and making chemical bonds. To develop new and green reactions, transition metal complexes based on cooperative ligands have been designed, and they have exhibited notable chemical reactivity.[2] These reactions can be facilitated by the cooperation of the noninnocent ligands and the metal center by undergoing reversible chemical and structural changes.

Milstein and co-workers have designed a new type of noninnocent ligand that supports metal–ligand cooperation that appears to involve an aromatization–dearomatization process of the pyridine- or acridine-based PNP and PNN "pincer" ligands. These complexes were reported to lead to the unusual X–H (X = H, C, O, N, and B) activation reactions and to environmentally benign catalysis involving dehydrogenation and hydrogenation reactions. Several reviews by Milstein and co-workers have appeared that give an overview of the experimental studies of these chemical reactions mediated by their designed complexes.[3]

The novel reactions supported by these metal–ligand complexes have attracted theoretical chemists to investigate their reaction mechanisms. The mechanisms are of interest just for the novelty of the reactions; in addition, an understanding of the mechanisms can help researchers to improve the current reactions and design new reactions. Many of the computational studies reported that the metal–ligand cooperation via reversible aromatization–dearomatization of ligands played an important role in some aspect of the reaction. Here, we review these theoretical studies by briefly introducing the related experimental work before discussing the reported computational mechanisms in details. Where several research groups proposed different mechanisms for the same reaction, we describe these mechanisms separately, recalculate their rate-determining steps

Received: November 25, 2014
Revised: February 2, 2015
Published: February 4, 2015

DOI: 10.1021/cs501875z
ACS Catal. 2015, 5, 1895–1913

by using functionals that are calibrated to produce the results close to those from the coupled cluster singles and doubles (CCSD) and CCSD(T), and then compare the new predictions to fully understand the most likely reaction pathway.

Analogous ruthenium complexes with aliphatic pincer ligands have been synthesized and used in catalysis.[4] Theoretical investigations of these complexes were reported,[4b−f] and the differences between the complexes with aliphatic and aromatic pincer ligands were compared.[4e] However, these types of ruthenium complexes are not the focus of this review because our focus is the ruthenium-based complexes with aromatic pincer ligands that undergo aromatization−dearomatization.

2. COMPUTATIONAL METHODS

When different computational methodologies are used by different research groups for the same reaction, it is often difficult to determine which group has predicted the correct mechanism if they are different. Therefore, benchmark calibrations were conducted by calculating the H_2 activation process with two simplified ruthenium complexes made by replacing the groups on the ligand arms with hydrogen atoms (eq 1 and eq 2 in Scheme 1).

Scheme 1. Activation of H_2 by the Simplified Ruthenium Complexes with Pyridine-Based PNN Ligand (eq 1) or with Pyridine-Based PNP Ligand (eq 2)

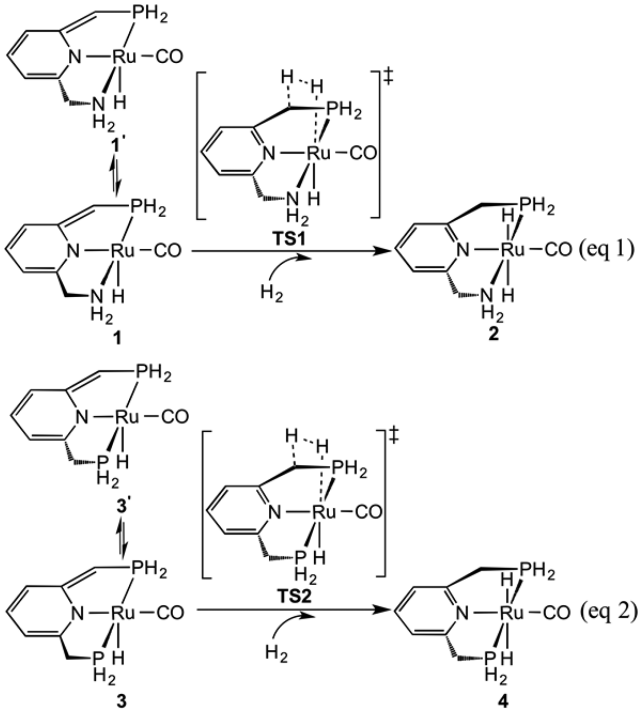

Using the basis set BS1, BS1 denotes an all-electron 6-31G(d,p)[5] basis for nonmetal atoms and SDD[6] ECP-basis for Ru. Geometries were optimized in the gas-phase with different functionals, including meta-GGA (generalized gradient approximation) and hybrid (with some true Hartree−Fock exchange) ones: M06L,[7] TPSS,[8] TPSS-D3,[8,9] B3LYP,[10] B3LYP-D3,[9,10] M06,[11] TPSSh,[8] and ωB97XD.[12] Their optimized geometries are quite similar to each other. According to the energy results in Table 1, their energy differences range from 0 to 6.8 kcal/mol, and the M06 functional produces the results that are nearly in the middle of the results from these functionals.

With the M06 functional, 10 basis sets were tested. The nonmetal atoms have the all-electron basis sets, 6-31G(d),[5] 6-31G(d,p),[5] 6-311G(d,p),[13] 6-311G(3df,2p), 6-311++G(d,p),[14] and the Dunning's correlation consistent basis set, cc-pVTZ.[15] The ruthenium atom has the basis sets with Stuttgart/Dresden ECPs (MDF28), involving SDD,[6] cc-pVDZ-PP, cc-pVTZ-PP, cc-pVQZ-PP, and aug-cc-pVTZ-PP.[16] The calculated results are collected in Table 2. According to Table 2, the results for M06/BS3 are very close to the results for the M06/BS4 with the diffuse function in the basis set, implying that the diffuse function has little effect on the energies. Moreover, the energies at the M06/BS3//M06/BS1 (energy calculation//geometry calculation) level are very close to those at the level of M06/BS3//M06/BS3 and are also close to those at the higher levels, from BS4 to BS10, with the deviations of <0.6 kcal/mol. Thus, the basis set BS3//BS1 is an acceptable comprise between calculation speed and accuracy.

Twenty DFT functionals were tested, and these functionals involve GGA, PBE;[17] meta-GGA, M06L,[7] TPSS,[8] and TPSS-D3;[8,9] hybrid-(meta-)GGA, B3LYP,[10] B3LYP-D3,[9,10] M06,[11] PBE0,[18] SOGGA11X,[19] BMK,[20] TPSSh;[8] long-range-corrected hybrid-(meta-)GGA, CAM-B3LYP,[21] ωB97XD,[12] ωB97X,[22] ωB97,[22] MN12SX,[23] HISSbPBE,[24] HSEH1PBE,[25] and LC-ωPBE;[26] and doubly hybrid B2PLYPD. These DFT calculations with the exception of B2PLYPD were conducted by using the basis set combination BS3//BS1. Calculations with the B2PLYPD functional and the coupled cluster singles and doubles (CCSD)[27] and CCSD(T)[28] used the geometries optimized at the level of M06/BS3, and BS11, an all-electron 6-311++G(d,p) for nonmetal atoms, and aug-cc-pVTZ-PP for Ru. The energetic results for the DFT functionals together with CCSD and CCSD(T) are shown in Table 3. According to Table 3, the LC-ωPBE functional produces results very close to those from CCSD(T). Moreover, several other functionals, TPSS, M06, and ωB97X-D, which were used in the previous computational studies, also produce results close to those from the CCSD and CCSD(T).

Recalculations for some reactions, in which the predictions of different workers varied, were conducted by using the functionals LC-ωPBE, TPSS, M06, and ωB97X-D. With these functionals, geometries of intermediates and transition states were optimized at the level of BS1. Harmonic vibration frequencies were calculated to identify intermediates with no imaginary frequency and transition states with only one imaginary frequency. Intrinsic reaction coordinate (IRC) calculations were further conducted when necessary.[29] The energetic results were further refined by single-point calculations with the SMD[30] solvent model in the experimentally reported solvent by using the same functional but with the higher-level basis set BS3. The harmonic frequencies obtained after geometry optimizations were used for the thermal and entropic corrections for enthalpies and free energies at 298 K and 1 atm. All the DFT calculations were conducted by using the Gaussian 09 program,[31] and the CCSD and CCSD(T) calculations were carried out with the Molpro program.[32]

3. COMPUTATIONAL MECHANISTIC STUDIES

Most of theoretical studies of the complexes synthesized by Milstein and co-workers are based on the ruthenium pyridine complexes.[33] These reactions involve the X−H (X = H, C, O, N, and B) activations,[34−41] dehydrogenative coupling reactions,[42−48] and hydrogenation reactions.[49−56] In addition, a theoretical study about the ruthenium acridine complex was also

DOI: 10.1021/cs501875z
ACS Catal. 2015, 5, 1895−1913

Table 1. Calculated Results for the Two Reactions, Eqs 1 and 2, by Using Different Functionals[a]

	eq 1				eq 2			
	1	1′	TS1	2	3	3′	TS2	4
M06L/BS1	0.0	0.0(7)	8.0	−20.3	0.0	0.0(2)	3.3	−25.0
TPSS/BS1	0.0	0.0(5)	8.4	−19.5	0.0	0.0(5)	3.6	−24.2
TPSS-D3/BS1	0.0	0.0(4)	6.7	−19.9	0.0	0.0(5)	1.8	−24.8
B3LYP/BS1	0.0	0.0(4)	13.5	−17.0	0.0	−0.0(1)	8.5	−22.2
B3LYP-D3/BS1	0.0	0.0(4)	11.5	−17.2	0.0	−0.0(02)	6.5	−22.5
M06/BS1	0.0	0.0(9)	9.8	−19.2	0.0	0.2	4.6	−24.7
TPSSh/BS1	0.0	0.0(9)	8.8	−20.2	0.0	0.0(5)	3.7	−25.4
ωB97XD/BS1	0.0	0.0(7)	10.0	−22.3	0.0	−0.0(3)	4.7	−28.1

[a]Values in kcal/mol are the SCF energies in gas phase. BS1 denotes the basis set compositions of all-electron 6-31G(d,p) basis for nonmetal atoms and SDD ECP-basis for Ru; values in the parentheses are the following decimal numbers.

Table 2. Calculated Results for the Two Reactions Eq 1 and Eq 2 with the M06 Functional in Different Basis Sets[a,b]

	eq 1				eq 2			
	1	1′	TS1	2	3	3′	TS2	4
M06/BS1	0.0	0.0(9)	9.8	−19.2	0.0	0.2	4.6	−24.7
M06/BS2	0.0	0.1	10.1	−20.5	0.0	0.2	5.3	−26.0
M06/BS3	0.0	0.1	11.0	−16.3	0.0	0.3	5.6	−21.9
M06/BS3//M06/BS2	0.0	0.1	10.9	−16.3	0.0	0.2	5.5	−21.9
M06/BS3//M06/BS1	0.0	0.1	10.9	−16.3	0.0	0.3	5.5	−21.9
M06/BS4	0.0	0.2	11.0	−16.0	0.0	0.2	5.7	−21.6
M06/BS5	0.0	0.1	11.4	−15.8	0.0	0.3	6.0	−21.3
M06/BS6	0.0	0.1	10.7	−16.4	0.0	0.3	5.4	−21.7
M06/BS7	0.0	0.1	10.4	−16.7	0.0	0.3	5.2	−22.0
M06/BS8	0.0	0.1	10.2	−16.9	0.0	0.2	4.9	−22.2
M06/BS9	0.0	0.0(4)	10.2	−16.9	0.0	0.3	4.9	−22.3
M06/BS10	0.0	0.1	10.5	−16.6	0.0	0.3	5.3	−21.7

[a]Values in kcal/mol are the SCF energies in gas phase. [b]Both energies and geometry optimizations are conducted at M06/BSx; BS2:6-31G(d)/SDD (Ru); BS3:6-311G(d,p)/SDD (Ru); M06/BS3//M06/BS1: single point energy at the M06/BS3 level based on the geometries at the M06/BS1 level; M06/BS3//M06/BS2: single point energy at the M06/BS3 level based on the geometries at the M06/BS2 level; BS4:6-31++G(d,p)/SDD (Ru); BS5:6-311G(3df,2p)/SDD (Ru); BS6:6-311G(d,p)/cc-pVDZ-PP (Ru); BS7:6-311G(d,p)/cc-pVTZ-PP (Ru); BS8:6-311G(d,p)/cc-pVQZ-PP (Ru); BS9:6-311G(d,p)/aug-cc-pVTZ-PP (Ru); BS10: cc-pVTZ/cc-pVTZ-PP (Ru); values in the parentheses are the following decimal numbers.

reported.[57] These theoretical studies are discussed in the following sections.

3.1. Mechanistic Studies for the X−H (X = H, C, O, N, and B) Activation. In 2006, Milstein and co-workers synthesized an iridium pincer complex **5**, (PNP)IrPh (PNP = 2,6-bis(di-*tert*-butylphosphinomethyl)pyridine), which was reported to activate H_2 to give the trans-dihydride complex **6** (Scheme 2).[58]

On the basis of the experimental studies, Li and co-workers investigated the reaction mechanism by DFT calculations using the B3LYP.[34] The singlet state surface was found to be more favorable than the triplet state surface; thus, their reported results are on the singlet surface. As shown in Scheme 3, the computed reaction mechanism involves three steps via the dearomatization−aromatization process of the PNP ligand. First, complex **5** is activated through the dearomatization of the PNP ligand by transferring one of its benzylic hydrogen atoms to the Ir center to form an iridium hydride intermediate **8** via **TS7**; second, complex **9** is formed by the coordination of H_2 to the Ir center in complex **8**; finally, the cleavage of H_2 by using the Ir atom and the dearomatized PNP ligand produces the trans-dihydride complex **6** via **TS10**. The first step is rate-determining, with a barrier of 35.9 kcal/mol for the B3LYP (**TS7**). The barrier is still high, 30−35 kcal/mol for several other functionals, TPSS, TPSSh, BMK, M05, and PBE. Thus, to explain the observed reaction at room temperature, they proposed that this step (the proton transfer) might occur via a hydrogen tunneling process.

Two other possible pathways were calculated to be unfavorable. In one, H_2 adds across the Ir−N bond of complex **9** via **TS11** to generate **12**. In the other channel, the H_2 oxidatively adds to the iridium atom of **5** and produces intermediate **13**; however, this channel is even higher in energy and can be excluded because the following processes from **13** to produce **6** are unfavorable.

Iron and co-workers studied this reaction by using the simplified complex $\mathbf{5^S}$ (^{t}Bu replaced by Me);[35] their reported mechanism is similar to that proposed by Li and co-workers. Moreover, they found that water molecules could facilitate the proton transfer step by bridging the gap the proton has to travel. On the basis of their reported results with M06, the barrier for the proton transfer without water molecule ($\mathbf{TS7^S}$) is 35.9 kcal/mol. The reaction barrier is decreased to 26.5 kcal/mol with the addition of one water molecule ($\mathbf{TS7^S\_H_2O}$ in Scheme 4). Two water molecules further lower the barrier to 20.7 kcal/mol ($\mathbf{TS7^S\_2H_2O}$ in Scheme 4) because the geometry of $\mathbf{TS7^S\_2H_2O}$ is less distorted than that of $\mathbf{TS7^S\_H_2O}$.

Two unfavorable possible pathways for this reaction proposed by Iron and co-workers are shown in Scheme 5. In one, a proton of the benzylic arm in $\mathbf{5^S}$ moves to the pyridine nitrogen atom (**14**), and then to the iridium atom ($\mathbf{8^S}$). In the other one, a α-hydride atom of the phenyl ring in $\mathbf{5^S}$ eliminates to the iridium

DOI: 10.1021/cs501875z
ACS Catal. 2015, 5, 1895−1913

Table 3. Calculated Results for the Two Reactions Eq 1 and Eq 2 with Different Functionals[a]

	eq 1				eq 2			
	1	1′	TS1	2	1	1′	TS1	2
PBE/BS3//PBE/BS1	0.0	−0.1	7.2	−17.7	0.0	0.1	2.3	−22.5
M06L/BS3//M06L/BS1	0.0	0.1	8.9	−18.1	0.0	0.1	3.9	−22.8
TPSS/BS3//TPSS/BS1	0.0	0.1	9.4	−17.0	0.0	0.1	4.3	−21.8
TPSS-D3/BS3//TPSS-D3/BS1	0.0	0.1	7.6	−17.5	0.0	0.1	2.5	−22.4
B3LYP/BS3//B3LYP/BS1	0.0	0.1	15.0	−14.2	0.0	0.1	9.8	−19.6
B3LYP-D3/BS3//B3LYP-D3/BS1	0.0	0.1	12.8	−14.4	0.0	0.1	7.6	−19.8
M06/BS3//M06/BS1	0.0	0.1	10.9	−16.3	0.0	0.3	5.5	−21.9
PBE0/BS3//PBE0/BS1	0.0	0.1	8.5	−19.2	0.0	0.1	3.1	−25.0
SOGGA11X/BS3//SOGGA11X/BS1	0.0	0.1	13.0	−17.0	0.0	0.1	7.7	−22.9
BMK/BS3//BMK/BS1	0.0	0.0(3)	11.5	−17.1	0.0	−0.1	6.3	−22.8
TPSSh/BS3//TPSSh/BS1	0.0	0.1	9.7	−17.7	0.0	0.1	4.5	−22.9
CAM-B3LYP/BS3//CAM-B3LYP/BS1	0.0	0.1	12.5	−18.6	0.0	0.1	7.1	−24.5
ωB97XD/BS3//ωB97XD/BS1	0.0	0.1	11.0	−19.6	0.0	0.0(3)	5.5	−25.5
ωB97X/BS3//ωB97X/BS1	0.0	0.1	11.6	−20.8	0.0	0.1	6.2	−26.8
ωB97/BS3//ωB97/BS1	0.0	0.2	11.8	−21.6	0.0	0.1	6.5	−27.6
MN12SX/BS3//MN12SX/BS1	0.0	0.3	13.9	−14.4	0.0	0.2	8.8	−19.8
HISSbPBE/BS3//HISSbPBE/BS1	0.0	0.2	10.4	−19.4	0.0	0.2	4.7	−25.4
HSEH1PBE/BS3//HSEH1PBE/BS1	0.0	0.1	8.7	−19.1	0.0	0.1	3.4	−24.7
LC-ωPBE/BS3//LC-ωPBE/BS1	0.0	0.2	9.8	−21.6	0.0	0.1	4.0	−28.2
B2PLYPD/BS11//M06/BS3	0.0	0.0	10.0	−19.5	0.0	0.1	4.3	−25.4
CCSD/BS11//M06/BS3	0.0	0.1	12.3	−20.9	0.0	0.1	6.5	−27.3
CCSD(T)/BS11//M06/BS3	0.0	0.0(4)	9.4	−21.8	0.0	0.1	3.4	−28.3

[a]Values in kcal/mol are the SCF energies in gas phase. Values in the parentheses are the following decimal numbers.

Scheme 2. Activation of H_2 by the Iridium Pincer Complex

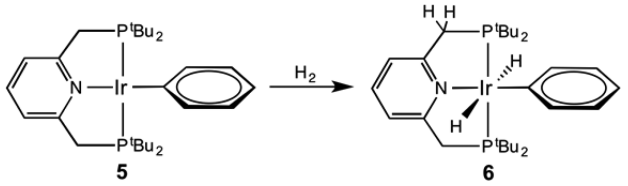

Scheme 3. Proposed Mechanism for the H_2 Activation by the Iridium Complex 5 in Benzene with the B3LYP by Li and Coworkers[a,34]

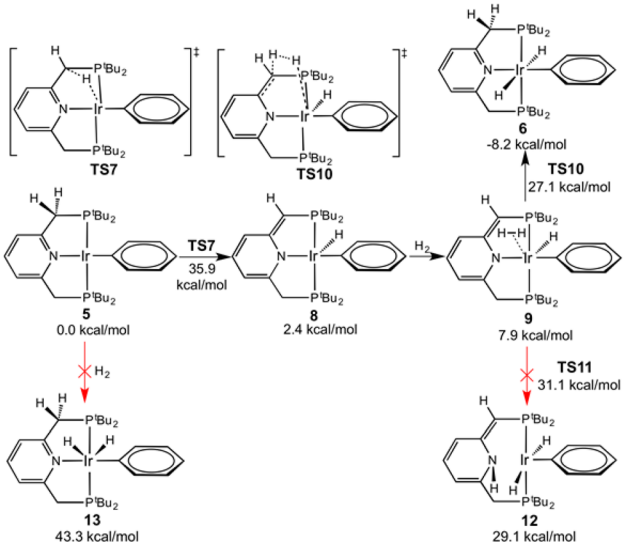

[a]Values are free energies.

Scheme 4. Proposed Transition States for the Proton Transfer with the Assistance of Water in Benzene with the B3LYP by Iron and Coworkers[a,35]

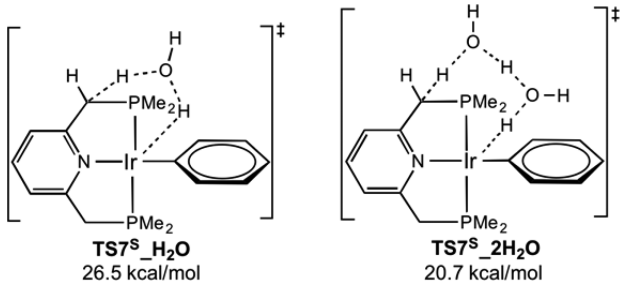

[a]Values are free energies relative to the separate 5^S and H_2O.

Scheme 5. Proposed Unfavorable Possible Pathways for the H_2 Activation by the Iridium Complex 5^S in Benzene with the B3LYP by Iron and Coworkers[a,35]

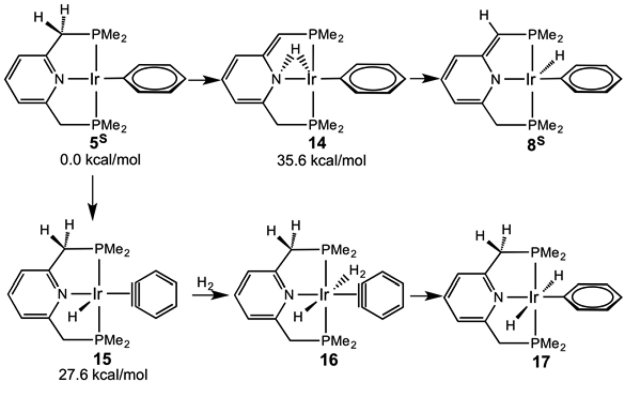

[a]Values are free energies.

DOI: 10.1021/cs501875z
ACS Catal. 2015, 5, 1895−1913

center to form complex **15**, followed by the H_2 coordination (forming **16**) and the H_2 cleavage to give complex **17**. However, the intermediates, **14** and **15**, are high in energy, 35.6 and 27.6 kcal/mol, respectively.

In 2010, Milstein and co-workers synthesized an iridium complex, (PNP)Ir(CH_2COCH_3) (PNP = 2,6-bis((di-*tert*-butylphosphino)methyl)pyridine), complex **18** in Scheme 6.[36]

Scheme 6. Proposed Mechanism for the Reactions of Complex 18 and H_2 or C_6H_6 in Benzene with the M06 by Milstein and Coworkers[a,36]

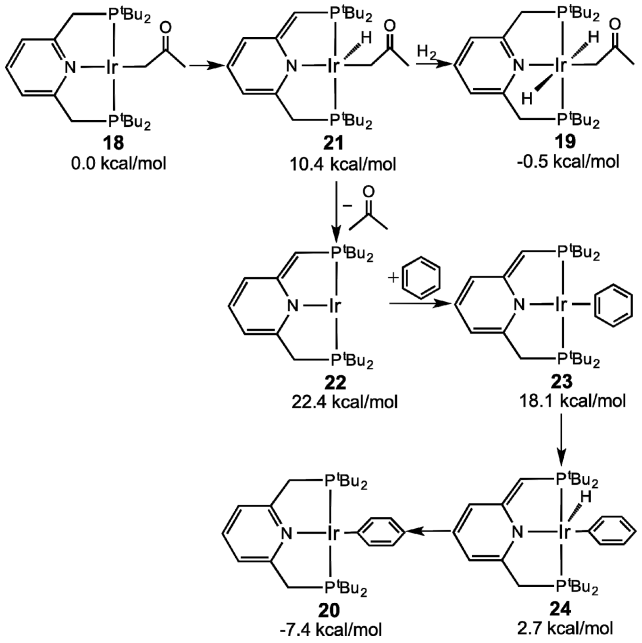

[a]Values are free energies.

Complex **18** was reported to react with H_2 and C_6H_6 to form the trans-dihydride complex **19** and the phenyl complex **20**, respectively. As shown in Scheme 6, the mechanism for the reaction of **18** and H_2 begins with the formation of the complex **21** with the dearomatization of the ligand via the proton transfer. Subsequently, H_2 binds to the iridium center of **21**, and is cleaved by the cooperation of the iridium atom and the unsaturated methylene arm to produce **19**. Two water molecules were found to facilitate the proton transfer process (**18** to **21**) by bridging the gap between the two sites. The reaction of **18** and C_6H_6 also starts with the formation of **21**, then the loss of acetone from **21** gives the complex **22**. The coordination of C_6H_6 to **22** forms **23**, followed by the C_6H_6's C−H bond activation to give **24**; rearomatization of **24** gives **20**. Two other routes where C_6H_6 adds to the iridium atoms of complexes **18** and **21**, respectively, were found to be unfavorable.

In the presence of CO, complex **18** again undergoes the elimination of acetone to form **25** with the dearomatization of PNP ligand (Scheme 7). On the basis of the experimental work, DFT calculations of the reaction mechanism show that the process begins with the formation of an intermediate, **26**, in which the acetonyl ligand is in the equatorial position by the coordination of CO to **18**. Rearrangement of **26** gives the analogue **27**, in which the acetonyl ligand is in the axial position. Elimination of acetone from **27** occurs via the water-assisted proton transfer from the methyl arm to the acetonyl; the barrier is only 2.7 kcal/mol relative to **27**. Possible pathways via the

Scheme 7. Proposed Mechanism for the Reactions of Complex 18 and CO in Benzene with the M06 by Milstein and Coworkers[a,36]

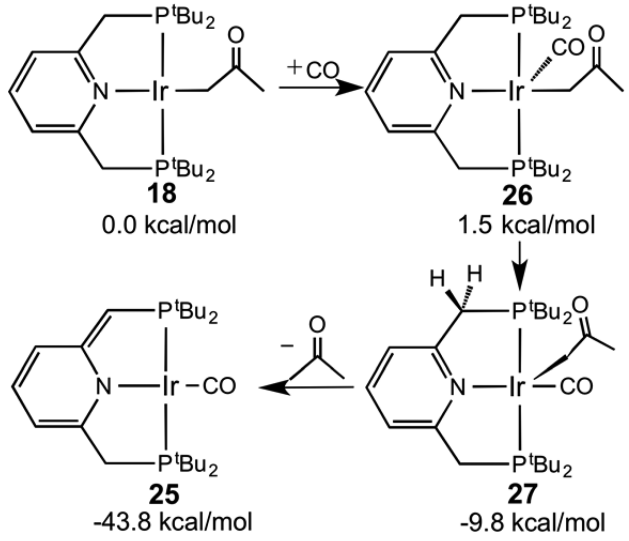

[a]Values are free energies.

formation of **21** are unfavorable because the formation of **21** has a barrier of 18.5 kcal/mol even with the assistance of two water molecules and **21** is higher than **18** by 10.4 kcal/mol.

In 2009, Milstein and co-workers reported a breakthrough method for the water splitting by using the PNN-based ruthenium pincer complex.[59] The sequential thermal-driven and light-driven steps in this reaction leads to the formation of H_2 and O_2; the mechanism has been investigated by several groups.[37−39,60] Yoshizawa and co-workers studied the reaction by using a model system **39′** (P^tBu_2 and NEt_2 replaced by PMe_2 and NMe_2, respectively) and proposed the mechanism in Scheme 8.[37] Addition of water to **39′** forms intermediate **28**, then a proton on the P side arm in **28** transfers to the hydride of the ruthenium center to form a dihydrogen complex **29** with the dearomatization of the ligand. One water molecule assists this proton transfer process with an activation barrier of 33.6 kcal/mol, and the resulting complex **29** is 20.1 kcal/mol relative to **28**. The release of H_2 from **29** leads to complex **30** with the dearomatization of the PNN lignd, and **30** can rearrange its ligand to form **31** by overcoming a barrier of 4.4 kcal/mol. Addition of H_2O to **31** gives **32**, and this process is exergonic by 8.7 kcal/mol.

The subsequent decomposition of H_2O by using the ruthenium atom and the PNN ligand results in the formation of the cis-dihydroxo complex **33** that leads to the formation of O_2 in the photolytic process. This step is exergonic by 9.6 kcal/mol and has a low barrier of 7.5 kcal/mol. It is possible that H_2O can bind to the vacant site trans to the OH group in **30**, forming complex **34**, followed by the H_2O's O−H bond cleavage by using the ruthenium center and the PNN ligand to form an aromatic trans-dihydroxo complex **35**. However, **35** cannot lead to the formation of O_2 or to isomerize to **33** because of the rigidity of its structure. The formation of the cis-dihydroxo complex **33** from **28** is slightly endergonic, and the release of H_2 from the reaction system is considered to drive this reaction to produce **33**. Alternatively to the release of H_2 from **28**, **28** may isomerize to its analogue in which the hydrogen atom on the P side arm is close

DOI: 10.1021/cs501875z
ACS Catal. 2015, 5, 1895−1913

Scheme 8. Proposed Mechanism for the Decomposition of H_2O To Release H_2 in Water with B3LYP by Yoshizawa and Coworkers[a,37]

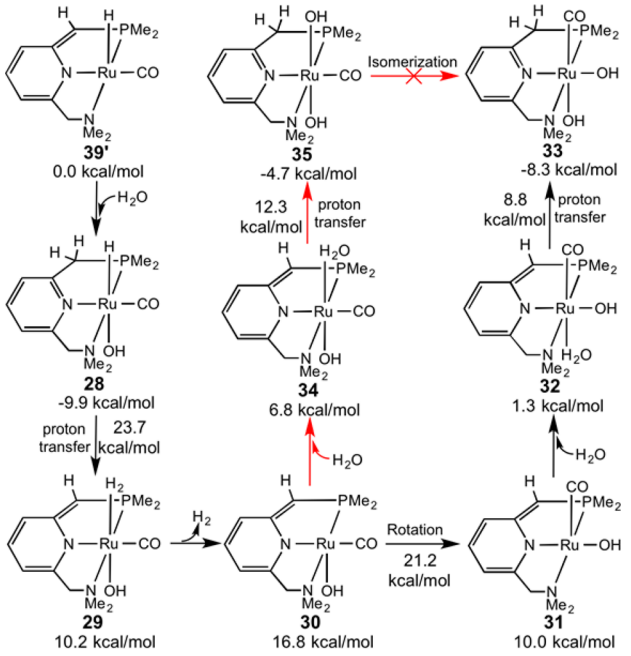

[a]Values are free energies.

to the hydroxyl group, followed by the proton transfer to the hydroxyl group to form H_2O. This process is reversible.

Almost at the same time, Yang and Hall investigated the reaction mechanism in much more detail by using the actual system with the TPSS functional.[38] The effects of aromatization and dearomatization of the PNN ligand were analyzed by comparing its possible isomers with the simplified model (R = H or Me), **36**, **37**, and **38** in Scheme 9. The aromatic isomer **36** is

Scheme 9. Isomers of the PNN Ligand

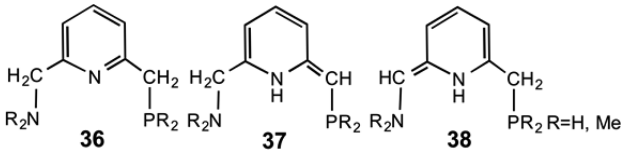

the most stable one, followed by the dearomatic isomer with the double bond on the P arm (**37**), and the dearomatic isomer with the double bond on the N arm (**38**) is the least stable one. Thus, the ruthenium complex with the more stable dearomatic ligand **37** rather than with its corresponding isomer **38** was synthesized. Scheme 10 shows the proposed pathways for the decomposition of water and the release of H_2. One water molecule binds the vacant site trans to the hydride in **39** to form an intermediate **40**. The water's O−H bond is split by using the ruthenium atom and the PNN ligand via **TS41**, which forms a more stable intermediate **42** that is lower by 0.2 kcal/mol than the separate **39** and water.

In contrast, **28** (the corresponding simplified model of **42**) is lower by 9.9 kcal/mol than the separate **39′** (the corresponding simplified model of **39**) and water (Scheme 8). The energy differences between them results from the steric effects of the substituents on their ligands; the water-cleaved product of the complex with the sterically bulky substituents (P^tBu_2 and NEt_2)

Scheme 10. Proposed Mechanisms for the Decomposition of Water and the Release of H_2 in Water with the TPSS by Yang and Hall[a,38]

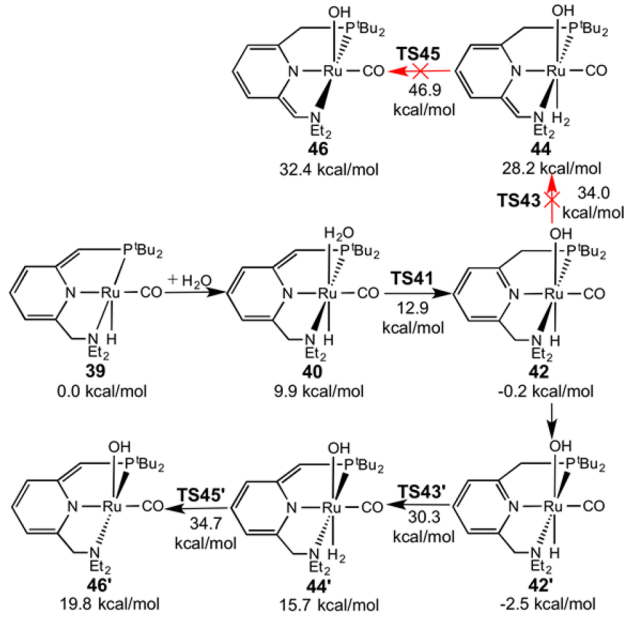

[a]Values are free energies.

is less stable than that for the simplified model with PMe_2 and NMe_2. Complex **42** then isomerizes to another more stable intermediate **42′**. A proton on the ligand's P arm in **42′** transfers to the hydride on the ruthenium center to form an unstable ruthenium hydrogen complex **44′** through a transition state **TS43′** with a barrier of 32.8 kcal/mol relative to **42′**. Finally, H_2 is released through a transition state **TS45′** with a barrier of 34.7 kcal/mol relative to the separate reactants, which forms an intermediate, **46′**. The rate-determining process is the release of H_2 through **TS45′**, and water plays no roles in this process. Alternatively, a proton of the ligand's N arm in **42** could transfer to the hydride of the ruthenium center through a transition state **TS43** to form **44**, followed by the release of H_2 to form **46**. However, these pathways are calculated to be less favorable. Time-dependent DFT calculations were conducted to understand the mechanism for the formation of O_2,[38,60] but these details are not the focus of this review.

In 2011, Sandhya and Suresh investigated the reaction again and proposed an alternative pathway for the release of H_2.[39] As shown in Scheme 11, water adds to the complex **39** to form another complex **47** where there are hydrogen bond interactions between the highly negative hydride ligand and the water molecule. Subsequently, water coordinates to the metal center, and simultaneously, the hydride and CO ligands change their orientations to form an intermediate **49**. Complex **49** then releases H_2. This step is rate-determining with a barrier of 32.56 kcal/mol (**TS50**). Finally, water adds to **51** to produce the cis-dihydroxo product **52** directly. The aromatization−dearomatization process of the PNN ligand does not participate in the H_2 release process according to this proposed mechanism.

According to the above discussions, two mechanisms for the release of H_2 were proposed. One is via **TS43′** (Scheme 10) involving the dearomatization−aromatization of the PNN ligand, and the other one is via **TS50** (Scheme 11) without the dearomatization−aromatization of the PNN ligand. Although the H_2 release transition state **TS45′** was rate-determining in the

DOI: 10.1021/cs501875z
ACS Catal. 2015, 5, 1895−1913

Scheme 11. Proposed Mechanism for the Water Splitting and the Release of H_2 in Water with the TPSS by Sandhya and Suresh[a,39]

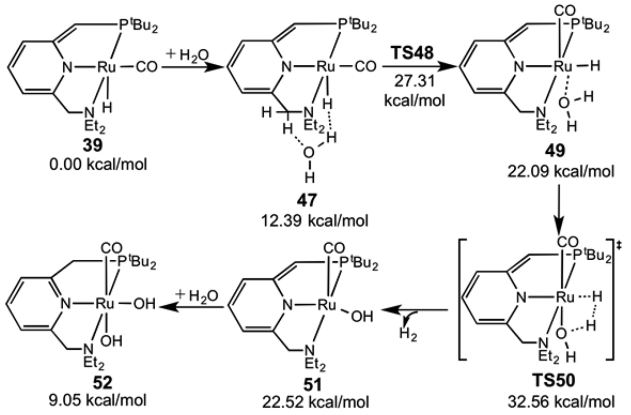

[a]Values are free energies.

calculations by Yang and Hall (Scheme 10), the recalculated results by using LC-ωPBE, TPSS, M06, and ωB97XD show that the H_2 formation transition state **TS43′** is higher than **TS45′**. Moreover, our recalculated results for the mechanism in Scheme 11 also show that the H_2 formation transition state **TS50** is higher than its corresponding H_2 release transition state. Thus, to investigate which mechanism is more favorable, we calculated the two H_2 formation transition states, **TS43′** and **TS50**. Water may facilitate the release of H_2 by bridging the hydrogen transfer gap via a transition state **TS43′_H₂O**. Table 4 shows the calculation

Table 4. Calculation Results for the Transition States TS43′, TS43′_H₂O, and TS50 for the Release of H_2[a]

functionals	TS43′	TS43′_H₂O	TS50
LC-ωPBE	41.7 [28.9]	38.6 [20.4]	38.9 [25.7]
TPSS	33.6 [20.7]	30.4 [12.3]	33.1 [19.9]
M06	41.5 [28.5]	38.8 [20.3]	37.5 [24.6]
ωB97XD	40.1 [27.8]	34.8 [16.7]	37.8 [24.7]

[a]Values in kcal/mol are the free energy and enthalpies (enthalpies are in the brackets) in water by using the methods discussed in the Computational Methods. Energies are relative to the separate reactants. The free energies for **TS43′_H₂O** are corrected by the adjustments for the standard-state concentration.[47]

results. The free energy may be overestimated.[61] According to Table 4, the barriers for **TS43′_H₂O** are lower than that for **TS43′**, showing that water facilitates the release of H_2. **TS43′_H₂O** is close to **TS50** with LC-ωPBE and is lower than **TS50** with TPSS and ωB97XD but is higher than **TS50** with M06. Thus, the two mechanisms are considered to compete with each other in this reaction.

In addition to the O−H bond activation, the dearomatized Ru complex with the PNP ligand was reported to be capable of activating N−H bond via the metal−ligand cooperation involving aromatization−dearomatization of the ligand.[40] DFT studies have confirmed a suitable transition state **TS53** (Scheme 12).

Cleavage of the B−H bond of boranes by the dearomatized ruthenium pincer complexes also involves metal−ligand cooperation.[41] The reaction favors the product in which the Lewis acidic boron atom adds to the benzylic arm of the ligand and hydride adds to the ruthenium atom.

Scheme 12. Proposed Transition State TS53 for the N−H Bond Activation by Using the Ru Complex[40]

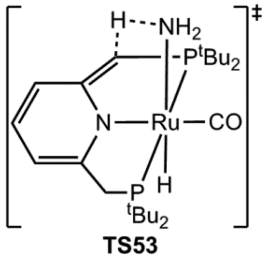

3.2. Mechanisms for the Dehydrogenative Coupling Reactions.

Milstein and co-workers have applied the ruthenium pincer complexes to catalyze the dehydrogenative coupling reactions to synthesize important compounds.[3c] In 2007, they reported the direct synthesis of amides from various amines and primary alcohols with the pincer complex Ru(II)-PNN (**39**).[62] On the basis of the experimental results, Milstein and co-workers proposed a mechanism in Scheme 13. The mechanism begins

Scheme 13. Mechanism for the Formation of Amides from Amine and Primary Alcohol Catalyzed by the Ruthenium Complex Proposed by Milstein and Coworkers

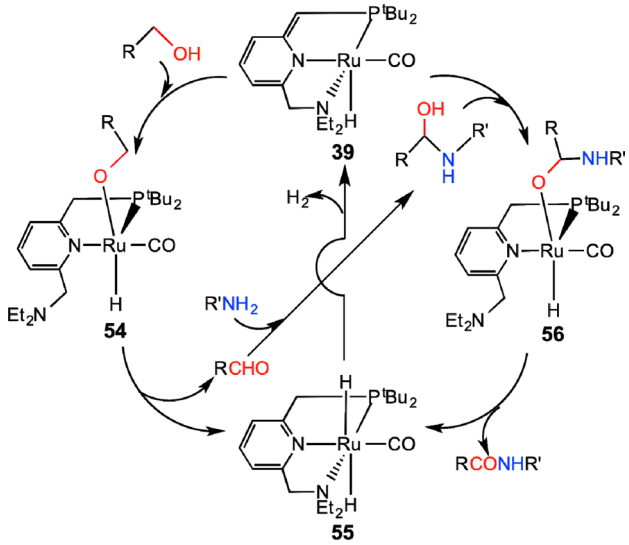

with the dehydrogenation of alcohol to form a trans-ruthenium dihydride complex **55** with the release of aldehyde by involving an intermediate **54**. Then the aldehyde couples with amine to give hemiaminal (RCH(OH)NHR′), followed by the dehydrogenation of hemiaminal to produce amide by involving an intermediate **56**. Finally, the trans-ruthenium dihydride complex **55** releases H_2 to regenerate the catalyst. The β-H elimination mechanism was proposed for the dehydrogenation processes.

On the basis of the experimental reaction, Wang and co-workers calculated the reaction mechanism in detail.[42] The calculated mechanism supports the mechanism proposed by Milstein and co-workers. For the dehydrogenation processes, Wang and co-workers proposed a bifunctional double hydrogen transfer mechanism (green lines in Scheme 14). It occurs stepwise via **TS57**, **58**, and **TS59**. **TS57** and **TS59** correspond to the alcohol's proton and hydrogen atom transferring to the dearomatized PNN ligand and ruthenium center, respectively. In the β-H elimination mechanism (red lines in Scheme 14),

DOI: 10.1021/cs501875z
ACS Catal. 2015, 5, 1895−1913

Scheme 14. Proposed Mechanisms for the Alcohol Dehydrogenation via Bifunctional Double Hydrogen Transfer Mechanism (in green) and β-H Elimination Mechanism (in red) in Toluene with the TPSS by Wang and coworkers[a,42]

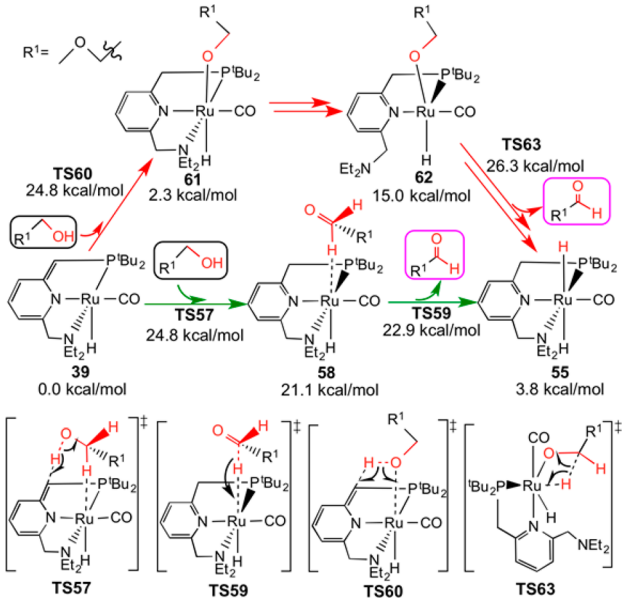

[a]Values are free energies.

alcohol adds to the catalyst **39** to form an intermediate **61** via **TS60**. The $-NEt_2$ arm in **61** opens to give an intermediate **62** with a vacant site on the Ru center, followed by the β-H elimination transition state **TS63** to release aldehyde and the coordination of $-NEt_2$ arm to produce **55**. The barrier for **TS63** is higher than those for **TS57** and **TS59**. Thus, the bifunctional double hydrogen transfer mechanism is calculated to be more favorable than the β-H elimination mechanism for the dehydrogenation of both alcohol and hemiaminal. Moreover, Milstein and co-workers indicated in their experimental study that the β-H elimination mechanism does not occur in the alcohol dehydrogenation.[63]

The coupling reactions between aldehyde and amine or alcohol to form hemiaminal **64** or hemiacetal **65** were mediated by alcohol that is used to bridge the proton transfer gap. An ester might be a possible byproduct because ester was observed without amine.[64] Scheme 15 shows that the coupling reactions favor forming the hemiaminal **64** rather than forming the hemiacetal **65** both thermodynamically and kinetically. This difference controls the reaction that selectively produces amide rather than ester; amide and ester are formed via the dehydrogenations of hemiaminal and hemiacetal, respectively. Another three unfavorable pathways for the coupling reactions are shown in Scheme 16: the direct coupling without any mediator via **TS68**, the coupling pathway mediated by amine via **TS69**, and the pathway mediated by the catalyst via **TS70** in which the cleaved amine group adds to the aldehyde. All the three pathways favor the formation of hemiaminal over hemiacetal.

Hemiaminal dehydrogenates via the double hydrogenation transfer mechanism to produce amide. Alternatively, it can also dehydrate to give imine. Scheme 17 shows three dehydration pathways: direct dehydration without any mediator via **TS71**, dehydration mediated by alcohol via **TS72**, and dehydration mediated by the catalyst via **TS73**. The barriers for these dehydration transition states are higher than those for the

Scheme 15. Coupling Reactions between Aldehyde and Amine or Alcohol To Form the Hemiaminal or Hemiacetal Mediated by Alcohol in Toluene with the TPSS by Wang and Coworkers[a,42]

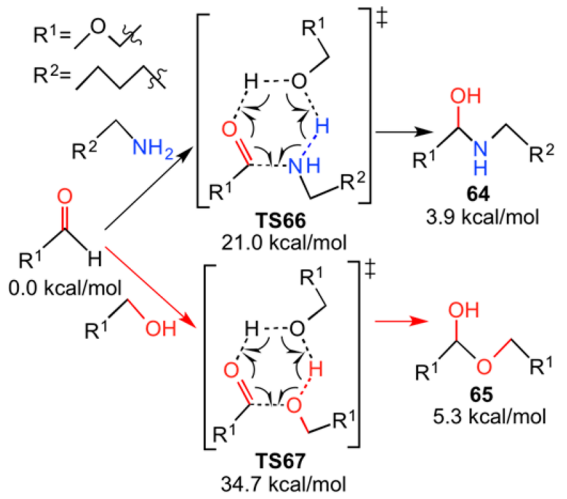

[a]Values are free energies.

Scheme 16. Proposed Transition States for the Coupling Reactions in Toluene with the TPSS by Wang and coworkers[a,42]

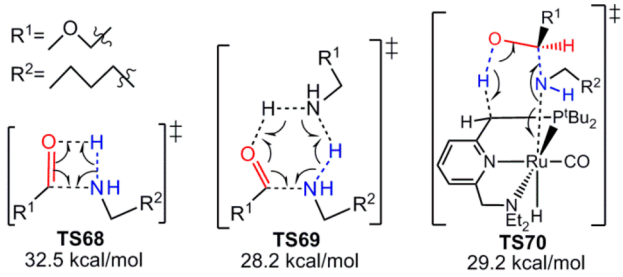

[a]Values are free energies relative to the separate reactants.

Scheme 17. Proposed Dehydration Transition States in Toluene with the TPSS by Wang and coworkers[a,42]

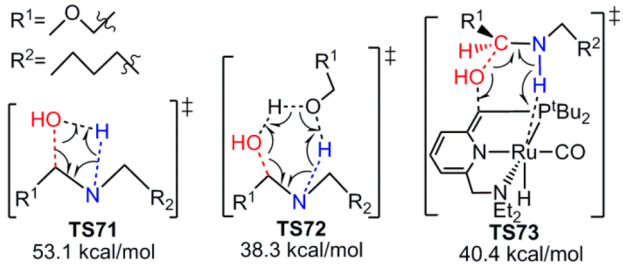

[a]Values are free energies relative to the separate reactants.

dehydrogenation transition states. This prediction is consistent with the experimental observation that the catalytic reaction produces amide rather than imine.

The formed ruthenium dihydride complex **55** should release H_2 to regenerate the catalyst **39**. Two pathways are possible: H_2 release process is direct without any mediator via **TS74**, or H_2 release process is mediated by an alcohol via **TS74_alcohol** (Scheme 18). **TS74_alcohol** is higher than **TS74**, showing that alcohol does not assist this process. A possible pathway via the

DOI: 10.1021/cs501875z
ACS Catal. 2015, 5, 1895−1913

Scheme 18. Proposed Mechanism for the Release of H_2 in Toluene with the TPSS by Wang and Coworkers[a,42]

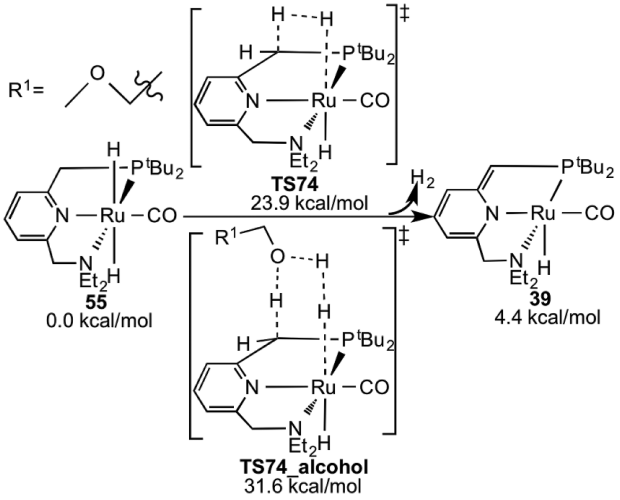

[a]Values are free energies.

transition state similar to **TS50** for the water splitting in Scheme 11 also is unfavorable.

In addition to the mechanism with the formation of the hemiaminal intermediate, other possible mechanisms without the formation of hemiaminal, as shown in Scheme 19, are

Scheme 19. Proposed Transition States without the Formation of Hemiaminal in Toluene with the TPSS by Wang and Coworkers[a,42]

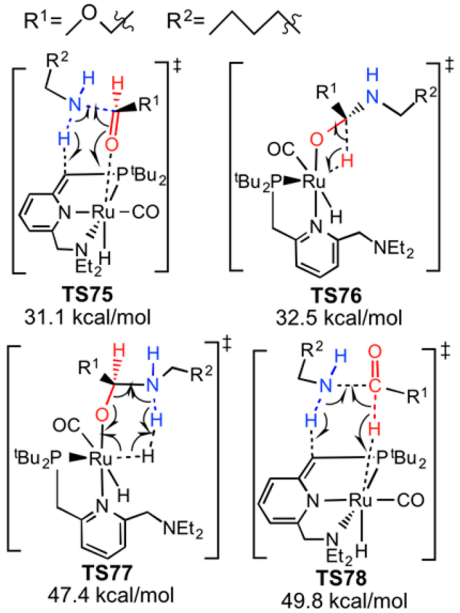

[a]Values are free energies relative to the separate reactants.

unfavorable. In one pathway, aldehyde and amine couples mediated by the catalyst via **TS75** to form a ruthenium alkoxide complex, followed by the β-H elimination (via **TS76**) to produce amide. The other two pathways occur through transition states **TS77** and **TS78**, respectively.

Lee and co-workers investigated the catalytic mechanism again and supported Wang and co-workers' finding that the bifunctional double hydrogen transfer mechanism is more favorable than the β-H elimination mechanism.[43] Moreover, they designed a new catalyst, which was predicted to have a higher catalytic reactivity, by the addition of an electron-donating substituent ($-NEt_2$) to the phenyl ring of the Milstein's catalyst (**79** in Scheme 20).

Scheme 20. A New Catalyst Designed by Lee and Coworkers[43]

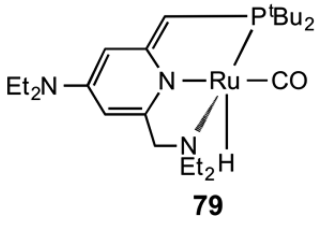

Almost at the same time, Zeng and Li reported their theoretical studies about the mechanism for this reaction.[44] The overall process in their proposed mechanism is similar to that proposed by Wang and co-workers; however, there are some differences with respect to the details of the dehydrogenation processes of the alcohol and hemiaminal. As shown in Scheme 21, the

Scheme 21. Proposed Mechanism for the Dehydrogenation of Alcohol in Toluene with the B3LYP by Zeng and Li[a,44]

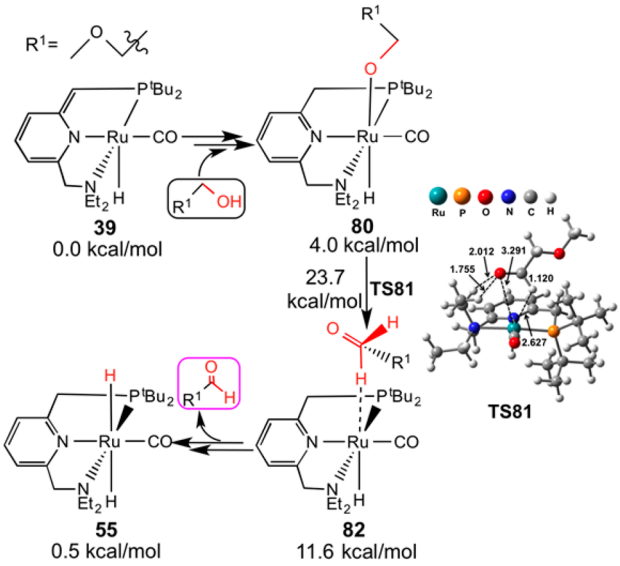

[a]Values are free energies.

mechanism for the dehydrogenation of alcohol proposed by Zeng and Li involves three steps: alcohol's O−H bond activation by the cooperation of the ruthenium center and the ligand to form intermediate **80**; rearrangement of the R^1CH_2O substituent in **80** to give an agostic complex **82** via transition state **TS81** where the oxygen and hydrogen atoms slip on the ruthenium center; transfer of the R^1CH_2O substituent's hydrogen atom to the ruthenium center to generate the trans-dihydride complex **55** with the release of aldehyde.

To investigate which of these two mechanisms is more favorable for the dehydrogenation of alcohol, we recalculated the transition state, **TS57**, rate-determining in the double hydrogen transfer mechanism, and **TS81**, rate-determining in the rearrangement mechanism. According to Table 5, **TS57** is always lower than **TS81** for all of these functionals; thus, the

DOI: 10.1021/cs501875z
ACS Catal. 2015, 5, 1895−1913

double hydrogen transfer mechanism is more favorable than the rearrangement mechanism.

Table 5. Calculated Transition States TS57 and TS81 for the Dehydrogenation of Alcohol[a]

functionals	TS57	TS81
LC-ωPBE	26.0 [10.7]	38.5 [23.2]
TPSS	22.6 [7.6]	36.6 [21.7]
M06	20.5 [4.6]	29.6 [14.3]
ωB97XD	16.0 [0.8]	27.3 [12.2]

[a]Values in kcal/mol are the free energy and enthalpies (enthalpies are in the brackets) in toluene by using the methods discussed in the Computational Methods. Energies are relative to the separate catalyst and alcohol.

Unlike the ruthenium PNN complex that can catalyze the synthesis of amide from amine and alcohol, the ruthenium PNP complex **83** was reported to catalyze the synthesis of imine from amine and alcohol.[65] Wang and co-workers also investigated this reaction theoretically and proposed that the mechanism is similar to that for the amide formation.[45] The differences between the two mechanisms are in the step for the hemiaminal dehydrogenation or dehydration. Moreover, water can catalyze the coupling reactions and the hemiaminal dehydration more effectively than alcohol can. As shown in Scheme 22, the alcohol dehydrogenation occurs via the bifunctional double hydrogen transfer mechanism via **TS84**, **85**, and **TS86** to form a ruthenium dihydride complex **87** with the release of aldehyde. The formation of hemiaminal is catalyzed by alcohol via **TS88** or catalyzed by water via **TS89** (Scheme 23). Scheme 24 shows the mechanism for the hemiaminal dehydration and dehydrogenation. The hemiaminal dehydration can be catalyzed by an alcohol via **TS90** or catalyzed by water via **TS91**. Alternatively, the hemiaminal could dehydrogenate mediated by the catalyst **83** to form amide via **TS92**. Although the hemiaminal dehydration to produce an imine is thermodynamically less favorable than the hemiaminal dehydrogenation to produce an amide, it is kinetically much more favorable. This kinetic preference determines the selectivity of imine over amide. Complex **87** cannot hydrogenate imine because the barrier for this process is very high.

Scheme 22. Proposed Mechanism for the Alcohol Dehydrogenation Catalyzed by the Ruthenium PNP Complex in Toluene with the TPSS by Wang and Coworkers[a,45]

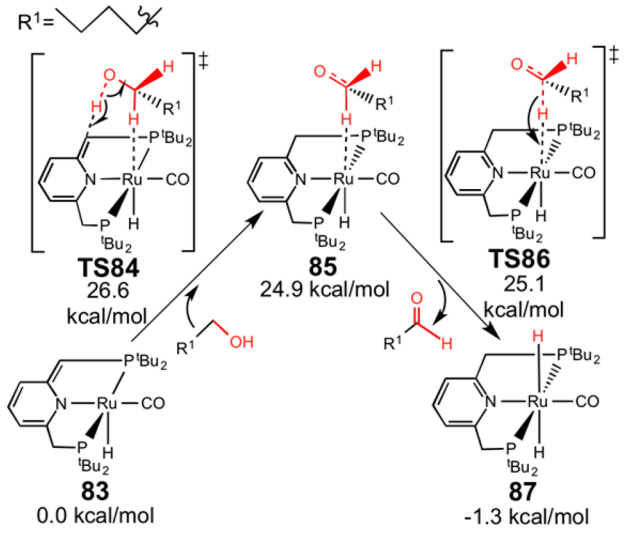

[a]Values are free energies.

Scheme 23. Proposed Mechanism for the Formation of Hemiaminal in Toluene with the TPSS by Wang and Coworkers[a,45]

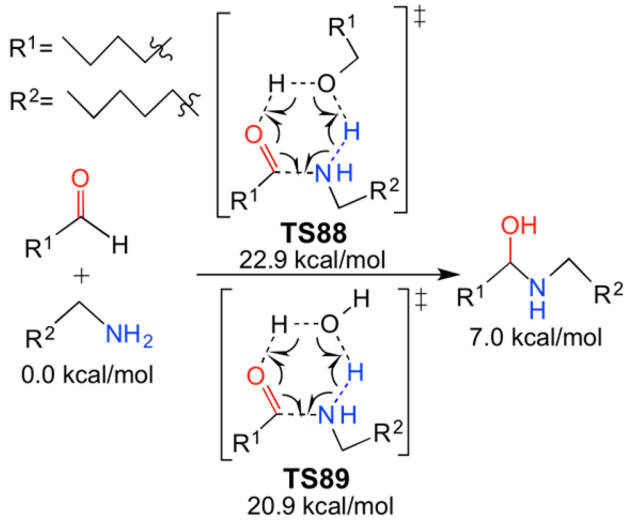

[a]Values are free energies.

Scheme 24. Proposed Mechanism for the Hemiaminal Dehydration and Dehydrogenation in Toluene with the TPSS by Wang and Coworkers[a,45]

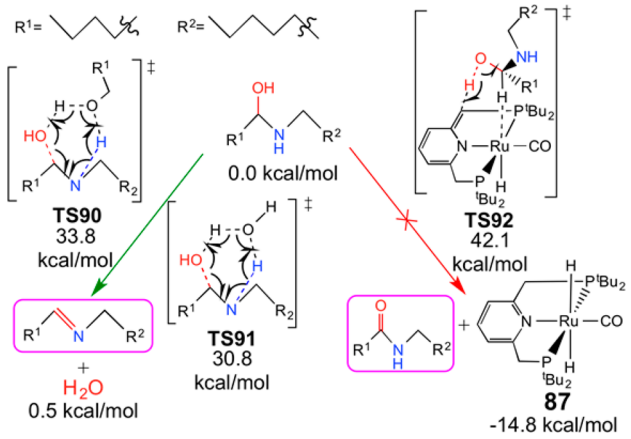

[a]Values are free energies.

For the synthesis of imine from alcohol and amine catalyzed by the ruthenium PNP complex **83**, Sandhya and Suresh proposed an alternative pathway by using the simplified complex **93** (^{t}Bu replaced by Me).[46] As shown in Scheme 25, the dehydrogenation of alcohol was proposed to proceed via transition state **TS94** which is similar to **TS50** for water splitting in Scheme 11 to form intermediate **95**. Subsequently, the CH_3CH_2O substituent's β-H atom eliminates to the ligand via transition state **TS96** to give intermediate **97**. Finally, the catalyst **93** can be regenerated via transition state **TS98**, in which the ligand's hydrogen atom migrates to the ruthenium center with the assistance of water. Two other pathways were calculated to be unfavorable: one involves the alcohol activation by the catalyst to form the ruthenium alkoxide complex that then releases H_2 from the trans

DOI: 10.1021/cs501875z
ACS Catal. 2015, 5, 1895−1913

Scheme 25. Proposed Mechanism for the Dehydrogenation of Alcohol with the TPSS by Sandhya and Suresh[a,46]

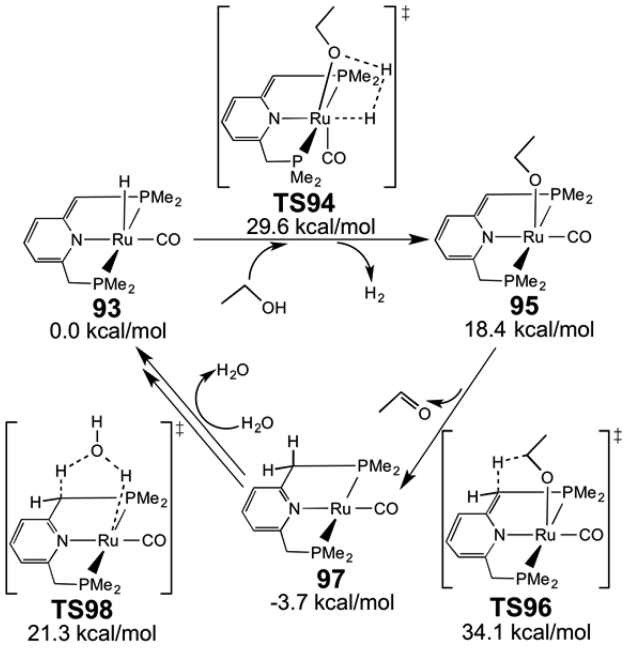

[a]Values are free energies.

position of the alkoxide group, and the other involves a β-H elimination mechanism with the dissociation of one P arm.

Scheme 26 shows the next step for the formation of the hemiaminal, in which the amine is cleaved by the catalyst **93** to form intermediate **100**, followed by the addition of the amino substituent to the aldehyde to give intermediate **102**. The

Scheme 26. Proposed Mechanism for the Formation of Hemiaminal with the TPSS by Sandhya and Suresh[a,46]

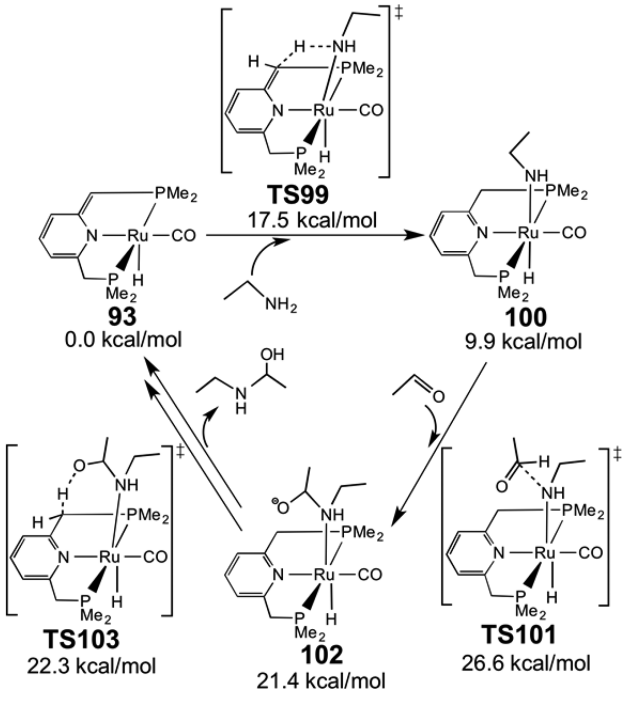

[a]Values are free energies

ligand's hydrogen atom migrates to the substituent, which leads to the hemiaminal via **TS103**. Subsequently, the hemiaminal dehydrates by following the pathway in Scheme 27. Transition

Scheme 27. Proposed Mechanism for the Dehydration of Hemiaminal with the TPSS by Sandhya and Suresh[a,46]

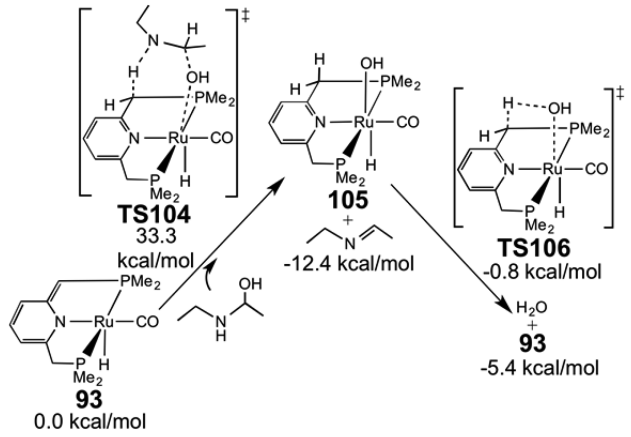

[a]Values are free energies

state **TS104** corresponds to the hemiaminal's proton and −OH group transferring to the ligand and the ruthenium center, respectively. Elimination of water from intermediate **105** regenerates the catalyst **93** via transition state **TS106**.

For the synthesis of imine from amine and alcohol, the two mechanisms discussed above are different. For the dehydrogenation of alcohol, we recalculated the two rate-determining transition states, **TS84** and **TS96′**. **TS96′** corresponds to transition state **TS96**, but **TS96′** uses the experimental system (the actual catalyst **83**, alcohol, and amine) that was also used in the calculations by Wang and co-workers. According to the calculated results in Table 6, **TS84** is always lower than **TS96′** for

Table 6. Calculated Transition States TS84 and TS96′ for the Dehydrogenation of Alcohol[a]

functionals	TS84	TS96′
LC-ωPBE	32.5 [16.8]	82.9 [76.6]
TPSS	27.6 [12.4]	51.0 [44.9]
M06	19.8 [6.5]	52.7 [47.4]
ωB97XD	20.2 [4.6]	63.1 [55.8]

[a]Values in kcal/mol are the free energy and enthalpies (enthalpies are in the brackets) in toluene by using the methods discussed in the Computational Methods. Energies are relative to the separate catalyst and alcohol.

all these functionals; thus, the dehydrogenation of alcohol favors the mechanism shown in Scheme 22. Moreover, **TS96′** is much higher (over 16 kcal/mol) than **TS96** because of the steric effects of the substituents ^{t}Bu in **TS96′** in comparison with Me in **TS96**. For the formation of hemiaminal, the mechanism shown in Scheme 26 is similar to the mechanism via **TS70** in Scheme 16. Moreover, the transition state **TS104** for the dehydration of hemiaminal in Scheme 27 is also similar to the transition state **TS73** in Scheme 17. **TS70** and **TS73** are calculated to be higher than the corresponding transition states mediated by the alcohol. Thus, considering the similarity between the ruthenium PNN complex **39** and ruthenium PNP complex **93**, the mechanisms

DOI: 10.1021/cs501875z
ACS Catal. 2015, 5, 1895−1913

shown in Schemes 23 and 24 should be more favorable than those in Schemes 26 and 27, respectively.

Using the bipyridine-based ruthenium complex **107**, in 2013, Milstein and co-workers reported a method to synthesize the carboxylic acid from alcohol and water.[66] With the ωB97X-D functional, Li and Hall investigated this reaction by calculating the catalytic mechanism for the formation of carboxylate from alcohols in basic aqueous solution.[47] On the basis of the experimental work, the mechanism was proposed to involve four steps (Scheme 28): alcohol dehydrogenates to aldehyde (step 1);

Scheme 28. Several Species Involved in the Catalysis Proposed by Li and Hall

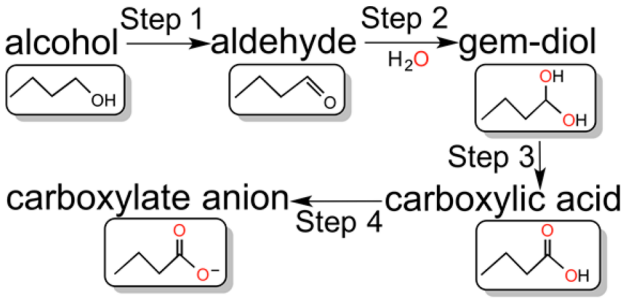

aldehyde couples with water to gem-diol (step 2); gem-diol dehydrogenates to carboxylic acid (step 3); and carboxylic acid deprotonates to carboxylate anion in basic conditions (step 4). The dehydrogenations of alcohol and gem-diol occur via the double hydrogen transfer mechanism, and the β-H elimination mechanism was found to be less favorable.

The proposed mechanism for the formation of the gem-diol is shown in Scheme 29. Water first adds to the catalyst **107** to form complex **109** via **TS108**, followed by the −OH group and H atom transferring to aldehyde in transition state **TS110** to generate the gem-diol. Two directions from the gem-diol are possible: dehydrogenation to the carboxylic acid over transition state **TS111** (forward) and decomposition into aldehyde and water over transition states **TS110** and **TS108** (backward). The backward process is more favorable than the forward process kinetically, which allows the rapid oxygen exchange between aldehyde and water. The addition of water to the regenerated catalyst **107** from **109** forms **109′**, resulting in repeated exchange of labeled and unlabeled oxygen atoms. This explains the experimental observations that both oxygen atoms of the carboxylic acid were from water.

Addition of the carboxylic acid to the catalyst **107** forms a carboxylic acid-addition complex **113** (R = $CH_3CH_2CH_2COO$). The base is reported to be capable of regenerating the catalyst **107** from both the carboxylic acid-addition complex and its precursor, ruthenium chloride complex. As shown in Scheme 30, the process involves two closely related, competitive pathways. In the solid-line pathway, complex **113** deprotonates over transition state **TS114**, followed by the dissociation of the anionic substituent over transition state **TS116**. In the broken-line pathway, the anionic substituent dissociates over transition state **TS117**, followed by the deprotonation over transition state **TS119**. Furthermore, the proposed mechanism for the reaction can explain the experimentally observed chemoselectivity for the formation of carboxylic acid rather than ester.[47]

Using the bipyridine-based ruthenium complex **107**, Milstein and co-workers reported a dehydrogenative coupling method to synthesize pyrroles from secondary alcohols and β−amino

Scheme 29. Proposed Mechanism for the Formation of the Gem-Diol in Water with the ωB97XD by Li and Hall[a,47]

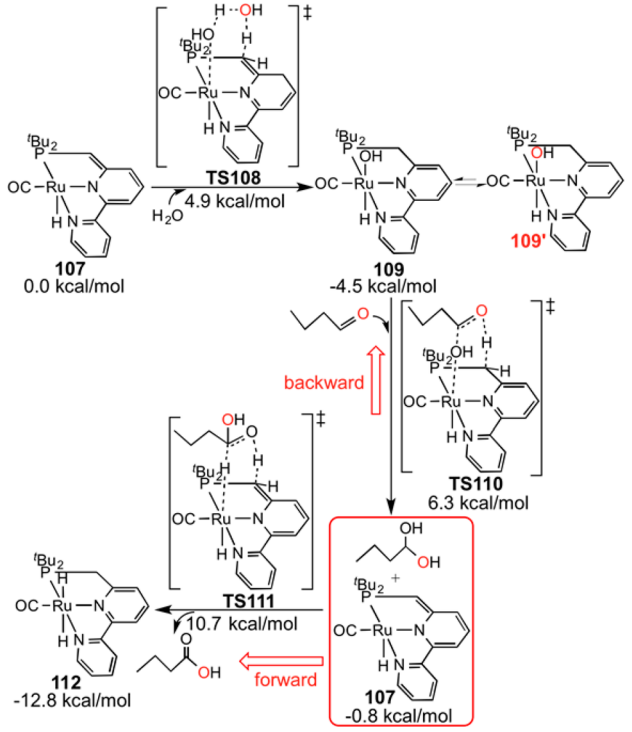

[a]Values are free energies.

Scheme 30. Proposed Mechanism for the Regeneration of the Catalyst from the Carboxylic Acid-Addition Complex or the Precursor Ruthenium Chloride Complex in Water with the ωB97XD by Li and Hall[a,47]

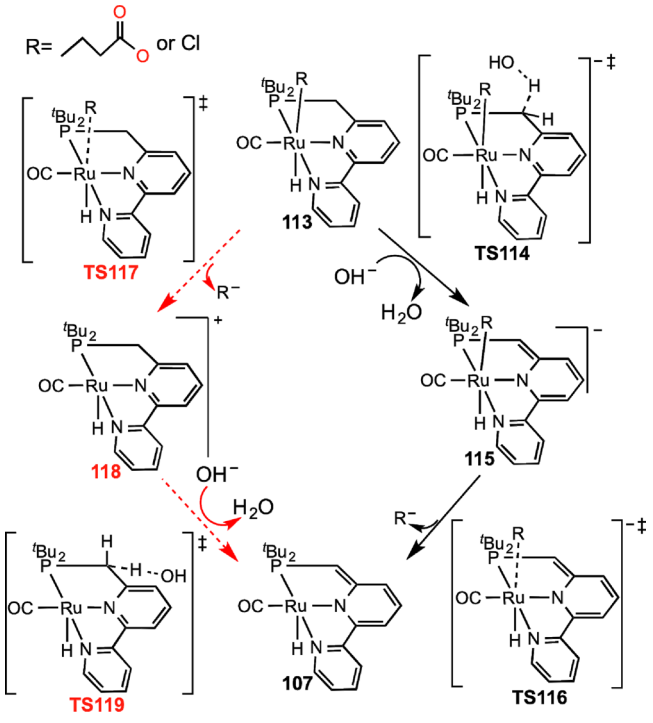

[a]Values are free energies.

alcohols.[67] On the basis of the experimental work, Wang and co-workers investigated the catalytic mechanism with DFT

DOI: 10.1021/cs501875z
ACS Catal. 2015, 5, 1895−1913

calculations.[48] The mechanism involves four steps. First, alcohol dehydrogenates to give ketone via transition state **TS120**, in which an additional alcohol behaves as an H-transfer shuttle (Scheme 31). The β-H elimination mechanism is calculated to be

Scheme 31. Proposed Transition State for the Dehydrogenation of Alcohol by Wang and Coworkers[48]

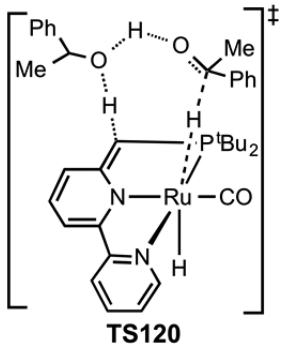

unfavorable. Second, ketone couples with alcohol to form an imine−alcohol intermediate **124** over transition states **TS121** and **TS123** under base (Scheme 32), which is more favorable

Scheme 32. Proposed Mechanism for the C−N Coupling of Ketone and β-Amino Alcohol To Form an Imine-Alcohol Intermediate by Wang and Coworkers[48]

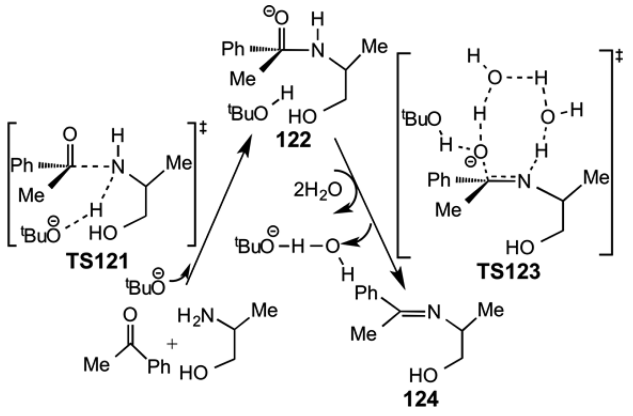

than that under neutral conditions. **TS123** with two water molecules is lower than those with only one and without a water molecule. The dehydrogenation of the imine−alcohol intermediate **124** forms imine−aldehyde **125**. Third, the imine−aldehyde **125** undergoes cyclization under base over transition states **TS126**, **TS128**, and **TS130** to form intermediate **131**, and subsequent intermolecular 1,2-H transfer leads to the pyrroles product **134** over transition states **TS132** and **TS133** (Scheme 33). The transition state **TS130** involving one water molecule as H-transfer shuttle is lower than the transition state without water. Moreover, the intermolecular H-transfer pathway over **TS132** and **TS133** is more favorable than the intramolecular 1,2-H transfer pathway. Finally, the ruthenium dihydride complex releases H_2 to regenerate the catalyst. In this mechanism, various proton-transfer (H-transfer) shuttles, such as alcohol and water, facilitate several H-transfer processes.

3.3. Mechanism for the Hydrogenation Reactions. By using their synthesized complexes, Milstein and co-workers have discovered hydrogenation reactions, the reverse of dehydrogenation, for ketones, amides, carbonates, and carbon dioxide. On

Scheme 33. Proposed Mechanism for the Cyclization under Base and the Intermolecular H-Transfer To Form the Pyrrole Product by Wang and Coworkers[48]

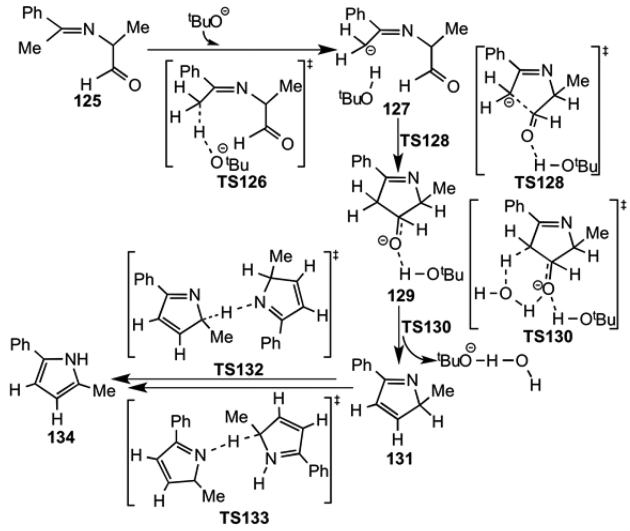

the basis of the experimental work, the mechanisms for the hydrogenation reactions were also investigated theoretically with DFT calculations.

In 2011, Milstein and co-workers synthesized an iron pincer complex that is applied for the ketones hydrogenation under mild conditions.[68] Using the ωB97X-D functional, Yang studied the hydrogenation mechanism with a simplified catalyst model **142** (^{i}Pr replaced by Me).[49] The mechanism in which the ketone inserts into the Fe−H bond (the reverse process of the β-H elimination) is found to have high barriers. Yang predicted a new mechanism (Scheme 34) that involves the formation of a trans dihydride complex **135**, the transfer of the hydride atom on the iron center to ketones to form a hydrido alkoxo complex, **137**. The dissociation of PhMeCHO$^-$ from **137** generates the

Scheme 34. Proposed Mechanism for the Hydrogenation Reactions in Ethanol with the ωB97XD by Yang[a,49]

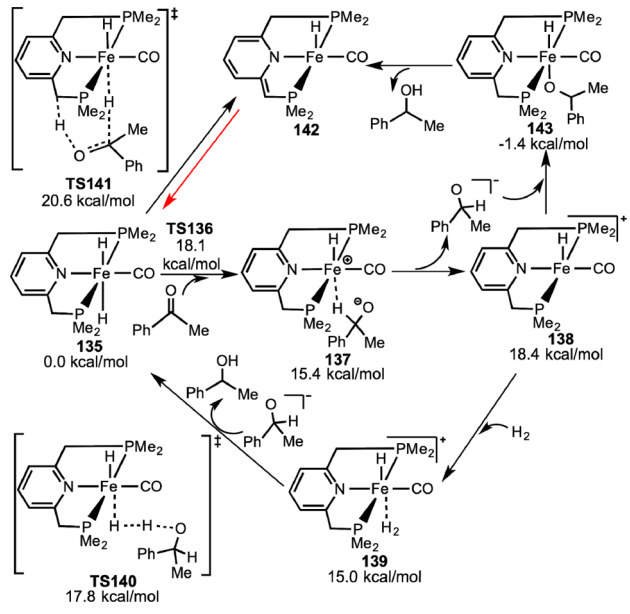

[a]Values are free energies.

DOI: 10.1021/cs501875z
ACS Catal. 2015, 5, 1895−1913

monocation **138**, then H_2 coordinates to **138** to form intermediate **139**, which is followed by the cleavage of H_2 with the participation of $PhMeCHO^-$ to regenerate **135** over transition state **TS140**. A pathway via the transition state **TS141**, in which the hydride on the iron center and a proton of the ligand transferring to ketone to generate **142** is proposed to be possible but is less favorable. The $PhMeCHO^-$ group may alternatively bind to **138** to form a stable complex **143**, which is followed by the elimination of PhMeCHOH to regenerate **142**. The solvent EtOH is proposed to stabilize **142** by reversibly binding to it. Moreover, EtOH plays an important role in the formation of **135**. In the pathway for the formation of **135** from **142**, EtOH adds to **142** to form an alkoxide complex, which then dissociates EtO^- to generate **138**, followed by the cleavage of H_2 with the cooperation of **138** and EtO^- via the transition state similar to **TS140**.

In 2010, Milstein and co-workers reported the hydrogenation of amides through the C−N bond cleavage by using the ruthenium bipyridine complex **107**.[69] In 2011, Cantillo investigated the mechanism by DFT calculations.[50] In one of his alternative mechanisms, the catalyst **107** reacts with H_2 to yield the ruthenium dihydride complex **112**. As shown in Scheme 35, the C−O cleavage can be achieved directly over the amide

Scheme 35. Proposed Mechanism for the Amides Hydrogenation with C−O Cleavage in THF with the M06 by Cantillo[a,50]

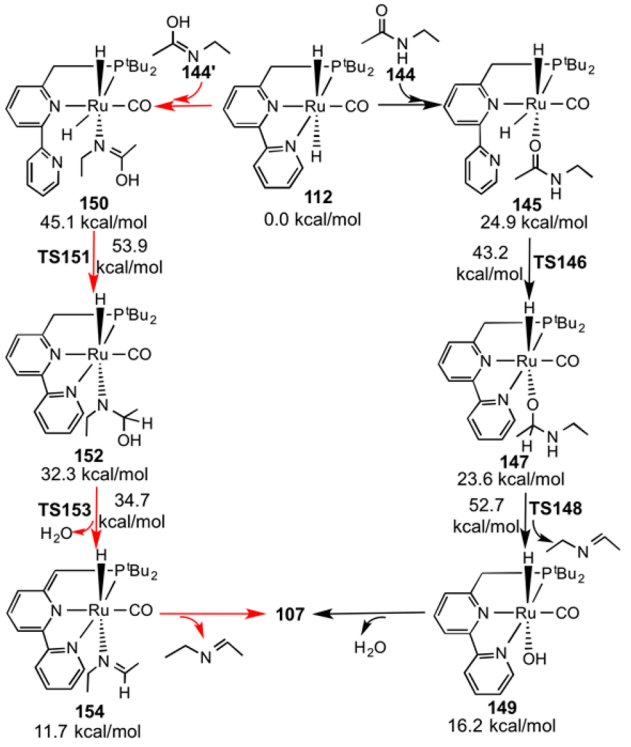

[a]Values are free energies.

substrate (**144**) or its imine tautomer (**144′**). The substrates **144** or **144′** first coordinate to **112** to give **145** or **150**, followed by the insertion of the hydride on the ruthenium center to one of the substrates to form **147** or **152**, respectively. The following C−O cleavage processes produce imine and H_2O. In the alternative to the hydride insertion transition state **TS146**, a proton on the ligand may transfer to the amide, but the barrier for this transition state is very high. Imine must be hydrogenated, and the proposed mechanism involves the hydride transfer intermediates **155** and **157** to produce amine (Scheme 36). The catalytic cycles for the

Scheme 36. Proposed Mechanism for the Imines Hydrogenation in THF with the M06 by Cantillo[a,50]

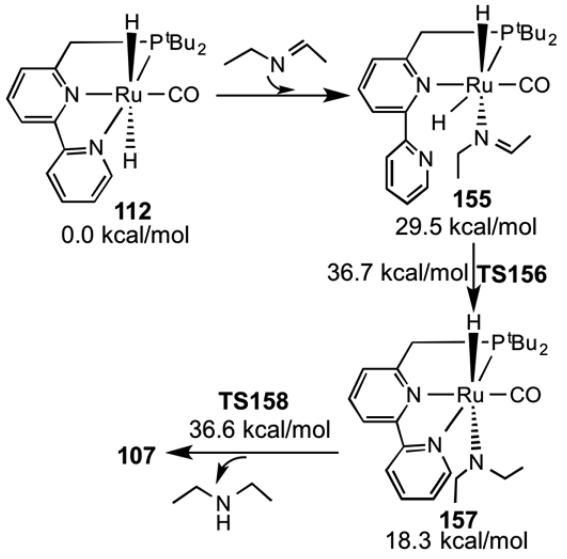

[a]Values are free energies.

C−N cleavage are shown in Scheme 37. When the intermediate **147** is formed, a proton on the ligand transfers to the amino group to form intermediate **160** with the release of amine. H_2 activation by **160** gives the ruthenium aldehyde complex **161**, which is followed by the aldehyde reduction to produce alcohol.

Scheme 37. Proposed Mechanism for the Amides Hydrogenation to Primary Amines and Alcohols with C−N Cleavage in THF with the M06 by Cantillo[a,50]

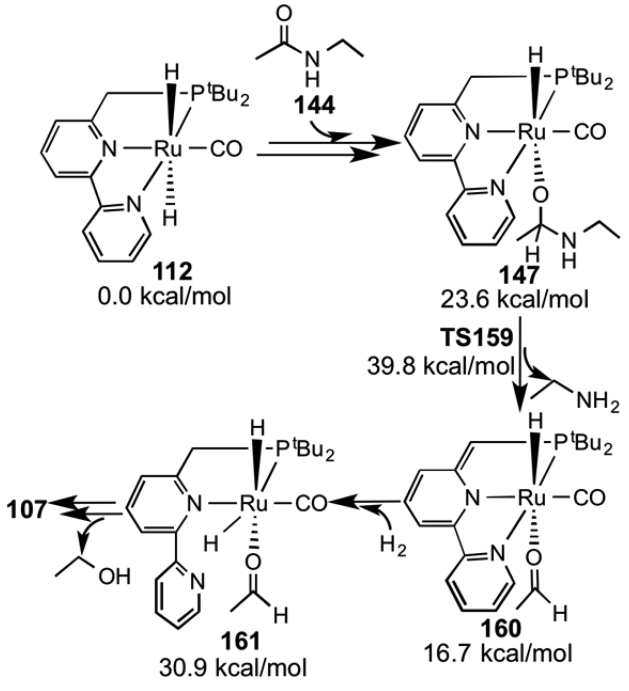

[a]Values are free energies.

DOI: 10.1021/cs501875z
ACS Catal. 2015, 5, 1895−1913

The observed selectivity could arise from the computed energy barrier for the C−N cleavage (Scheme 37), being 10 kcal/mol lower than that for C−O cleavage (Scheme 35); however, the barriers for both the mechanisms are very high. The following discussions about the mechanism for the hydrogenation of carbonate will give some insights into an alternative mechanism for this reaction.

In 2011, Milstein and co-workers reported the hydrogenation of dimethyl carbonate to form methanol catalyzed by ruthenium PNN complex, affording an indirect transformation of CO_2 to methanol.[70] On the basis of the experimental work, several groups investigated the catalytic mechanism with DFT calculations. Wang and co-workers investigated the reaction, and their proposed mechanism includes three steps, each one involving the catalyst: hydrogenation of dimethyl carbonate to methyl formate and methanol; hydrogenation of methyl formate to formaldehyde and methanol; and hydrogenation of formaldehyde to methanol.[51] The first two hydrogenation steps are similar. The proposed mechanism for the hydrogenation of dimethyl carbonate is shown in Scheme 38, which involves

Scheme 38. Proposed Mechanism for the Hydrogenation of Dimethyl Carbonate to Methyl Formate and Methanol in 1,4-Dioxane with the TPSS by Wang and Coworkers[a,51]

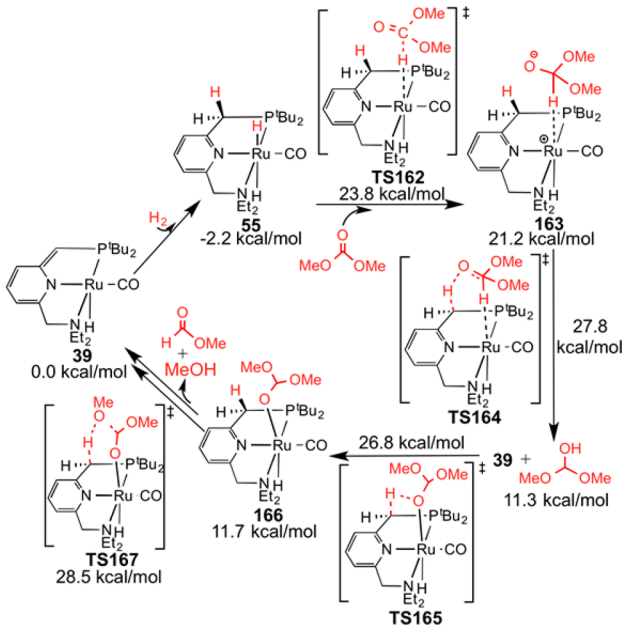

[a]Values are free energies.

hydrogen activation (from **39** to **55**), formation of a hemiacetal intermediate via stepwise hydrogen transfer to dimethyl carbonate via **TS162**, **163**, and **TS164**, and decomposition of the hemiacetal to methanol via **TS165**, **166**, and **TS167**. One possible pathway for the directly formation of **166** from **163** via the transition state where the $(MeO)_2CHO^-$ group's hydrogen and oxygen atoms rearrange on the ruthenium atom has a high barrier. Moreover, hydrogenation via carbonyl insertion into the Ru−H bond is less favorable than the stepwise hydrogen-transfer mechanism via **TS162**, **163**, and **TS164**. In addition to the catalyst **39**-mediated decomposition of hemiacetal, two other pathways that do not involve the catalyst were found to be unfavorable: intermolecular H-exchange between two hemiacetals and methanol acting as a proton-transfer bridge to facilitate intramolecular hydrogen transfer from the OH group to the OMe group.

Comparing the three steps, the first step is the most difficult, the second one is less difficult, and the third one is the easiest both kinetically and thermodynamically. A proposed mechanism[70] in which the methyl formate formed in the first step still coordinates to the catalyst **39**, followed by the hydrogen activation, was calculated to have a very high barrier.

Almost at the same time, Yang investigated this reaction and proposed a mechanism that involves three similar steps.[52] The major difference between the two mechanisms is the formation of the ruthenium alkoxide complex **166**. According to the Yang's mechanism (Scheme 39), the intermediate **163** formed via the

Scheme 39. Proposed Mechanism for the Formation of Complex 166 in THF with the ωB97XD by Yang[a,52]

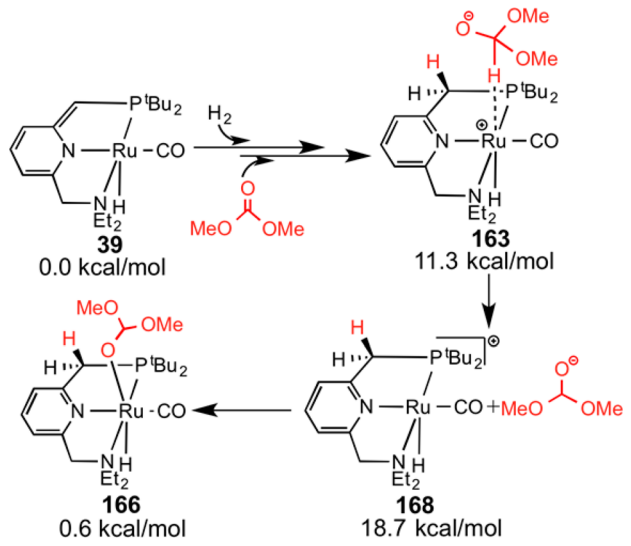

[a]Values are free energies.

hydride transfer process dissociates the $(MeO)_2CHO^-$ group to form the monocation **168**, followed by the reassociation of $(MeO)_2CHO^-$ group to **168** to form complex **166**. However, Yang failed to locate the transition state for this association process. The third step of the hydrogenation of formaldehyde occurs via the mechanism, similarly to that for the hydrogenation of dimethyl carbonate via the dissociation and reassociation of CH_3O^-, followed by a proton on the ligand transferring to the CH_3O^- group to form methanol.

A third group, Hasanayn and co-workers, also studied this reaction for the hydrogenation of dimethyl carbonate. They proposed an alternative metathesis pathway that is shown in Scheme 40 by using the simplified complex **169** (Et replaced by Me).[53] The metathesis mechanism in which a hydride and an alkoxide switch their coordination on the metal center was reported previously to explain the mechanism for the ester hydrogenation and transesterification.[54] Moreover, they used the metathesis mechanism to explain the dehydrogenative coupling reactions of amines with alcohols or esters to produce carboxamides.[55] As shown in Scheme 40, the metathesis mechanism for the hydrogenation of dimethyl carbonate involves (i) the hydride in the ruthenium dihydride complex **170** transfer to the dimethyl carbonate to give complex **172**, where the C−H bond of the $[OCH(OMe)_2]^-$ anion faces the metal center over transition state **TS171**, and (ii) the $[OCH(OMe)_2]^-$ anion's

DOI: 10.1021/cs501875z
ACS Catal. 2015, 5, 1895−1913

Scheme 40. Proposed Mechanism for the Hydrogenation of Dimethyl Carbonate to Methyl Formate and Methanol in THF with the M06 by Hasanayn and Coworkers[a,53]

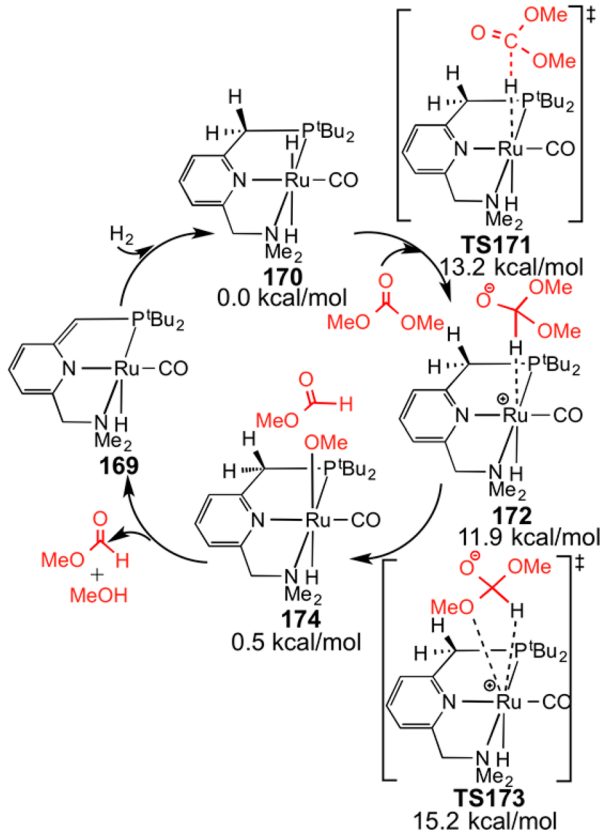

[a]Values are free energies.

rearranging on the ruthenium center with the cleavage of C−OMe over transition state **TS173** to give complex **174**. Two alternative pathways shown in Scheme 41 were calculated to be less favorable: (iii) metathesis via the transition state **TS175**, which is different from **TS173** in the orientation of the $[OCH(OMe)_2]^-$ group, occurs stepwise through **176** and a C−OMe cleavage transition state **TS177**, and (iv) carbonyl group insertion into the Ru−H bond via transition state **TS178** and β-alkoxide elimination via transition state **TS180**.

In their reports, the energetics of the metathesis pathway shown in Scheme 40 are calculated to be lower than the pathway via the protonation of the methoxy group to eliminate methanol over transition state **TS167** in Scheme 38, considered as favorable by the other investigators, Yang[52] and Wang and co-workers.[51] Hasanayn and co-workers suggested that an indirect metathesis pathway in which the intermediate **172** dissociates into the $(OMe)_2CHO^-$ anion and the monocation followed by the reassociation to form complex **176** might be even lower in energy.

Unlike the mechanisms of Yang and Wang and co-workers, in which the first step is rate-determining, in the mechanism of Hasanayn and co-workers, the metathesis transition state, **TS181**, for the hydrogenation of methyl formate becomes rate-determining (Scheme 42). Inclusion of one methanol molecule as a hydrogen-bond donor was proposed to facilitate the metathesis pathway over the transition state **TS182** (**TS173**_MeOH) and the elimination of methanol through the protonation transition state **TS183** (**TS167^S**_MeOH) (Scheme

Scheme 41. Unfavorable Mechanism for the Hydrogenation of Dimethyl Carbonate to Methyl Formate and Methanol in THF with the M06 Proposed by Hasanayn and Coworkers[a,53]

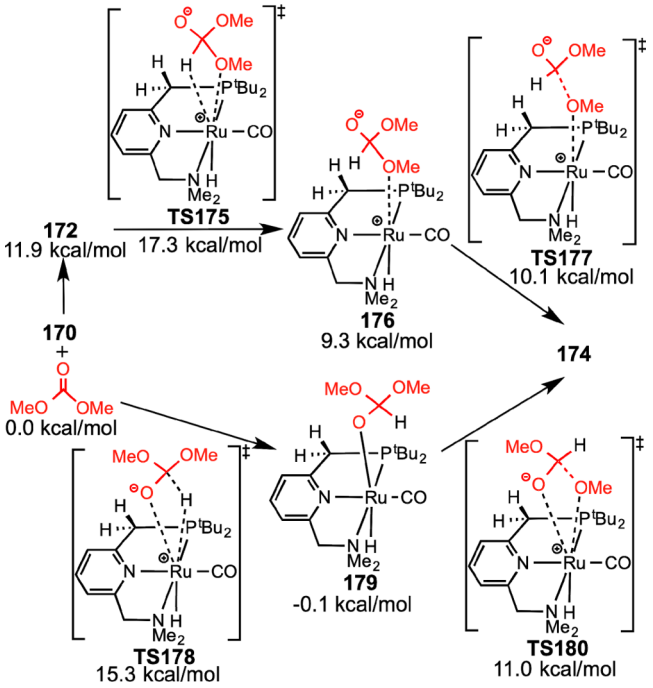

[a]Values are free energies.

Scheme 42. Proposed Transition States TS181, TS182 (TS173_MeOH), and TS183 (TS167^S_MeOH) in THF with the M06 by Hasanayn and Coworkers[a,53]

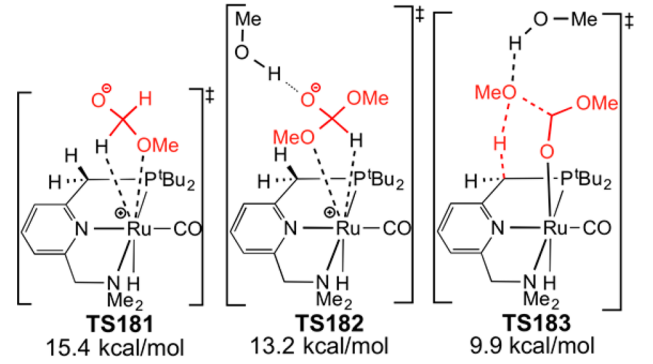

[a]Values are free energies.

42). **TS167^S** corresponds to the transition state **TS167** (Et replaced by Me).

Because several mechanisms were proposed to explain the hydrogenation of dimethyl carbonate, we recalculated several important species involved in these mechanisms. These new computational results, shown in Table 7, compare the energies of several rate determining TSs: transition state **TS167** in the metal−ligand cooperation mechanism (Scheme 38), the dissociation process to form the $(MeO)_2CHO^-$ group and the monocation **168** (Scheme 39), the slippage transition state **TS173′**, the metathesis transition state **TS181′**, and its methanol-assisted counterparts **TS182′** (**TS173′**_MeOH) and **TS183′** (**TS167**_MeOH, Schemes 40−42). In our recalculations, we used the actual catalyst system for **TS173′**, **TS181′**, **TS182′**, and **TS183′** rather than the simplified ligand used for

DOI: 10.1021/cs501875z
ACS Catal. 2015, 5, 1895−1913

Table 7. Calculated Results for TS167, 168, TS173′, TS181′, TS182′ (TS173′_MeOH), and TS183′ (TS167_MeOH) for the Hydrogenation of Dimethyl Carbonate[a]

	LC-ωPBE	TPSS	M06	ωB97XD
TS167	29.8 [6.7]	29.8 [7.0]	24.7 [−0.5]	18.3 [−4.9]
168 + $(MeO)_2CHO^-$	27.7 [20.2]	30.3 [23.7]	29.8 [22.0]	31.6 [22.5]
TS173′	32.3 [8.9]	36.3 [13.3]	25.8 [1.4]	21.9 [−1.3]
TS181′	29.9 [6.7]	33.9 [11.1]	25.0 [0.9]	21.1 [−1.9]
TS182′ (**TS173′**_MeOH)	28.6 [−3.5]	35.9 [2.8]	23.7 [−12.1]	15.9 [−16.6]
TS183′ (**TS167**_MeOH)	20.9 [−13.5]	28.9 [−3.5]	19.3 [−15.6]	12.1 [−21.5]

[a]Values in kcal/mol are the free energy and enthalpies (enthalpies are in the brackets) in THF by using the methods discussed in the Computational Methods. Energies are relative to the separate reactants.

TS173, **TS181**, **TS182**, and **TS183**. According to the results in Table 7, the transition states with the actual catalyst system (**TS173′**, **TS181′**, **TS182′**, and **TS183′**) are higher than those with the simplified ligand (**TS173**, **TS181**, **TS182**, and **TS183**), which shows the steric effects of the ligands' substituents. Moreover, when the actual catalyst is used in the calculations, the hydrogenation of methyl formate is not rate-determining because **TS181′** is lower than **TS173′** for these four functionals. **TS182′** (**TS173′**_MeOH) and **TS183′** (**TS167**_MeOH) are lower than **TS173′** and **TS167**, respectively, showing that MeOH facilitates the two pathways. Considering that the barriers for these transition states are only different by several kilocalories per mole, the three pathways should be considered as competitive with each other in the catalytic reaction. These mechanisms may give some insights into the understanding of the mechanism for the hydrogenation of amide proposed by Cantillo (Schemes 35−37).[50]

In 2011, Milstein and co-workers developed an iron pincer complex that is able to efficiently hydrogenate carbon dioxide under low pressures and with high turnover numbers.[71] This is consistent with Yang's computational prediction by using the DFT calculations.[56] According to these calculations (Scheme 43), the reaction begins when a CO_2 molecule added to one of the hydrides in complex **184** over a hydride transfer transition state **TS185** to form intermediate **186**. Dissociation of $HCOO^-$ from **186** gives a monocation **187**, followed by H_2 binding to the vacant position in **187** and H_2 cleavage by OH^- without the involvement of the PNP ligand over transition state **TS188** to regenerate **184**. The other two pathways via the coordination of $HCOO^-$ and OH^- to the vacant position in **187** are calculated to be less favorable.

In addition to the iron pincer complex for the hydrogenation of CO_2, the ruthenium complex with the dearomatized PNP-pincer ligand was also reported to activate CO_2.[72] However, both experimental and computational studies show that the reaction occurs reversibly by adding CO_2 to the ruthenium center and the unsaturated PNP-pincer ligand, which forms new C−C and Ru−O bonds.

3.4. Mechanisms for the Reactions of an Acridine-Based Ruthenium Pincer Complex. In addition to the pyridine-based complexes, Milstein and co-workers synthesized an acridine-based PNP-pincer ruthenium complex.[73] Hofmann and co-workers investigated the mechanism of the amination of alcohols with ammonia catalyzed by the ruthenium acridine complex **189** both experimentally and by DFT calculations.[57] The proposed initiation mechanism is shown in Scheme 44. Dissociation of Cl^- and coordination of MeO^- gives complex **190**, followed by the dearomatization via hydride transfer to the acridine ring's C9 position to form intermediate **191** that then releases aldehyde to generate complex **192**. The proposed

Scheme 43. Proposed Mechanism for the Hydrogenation of Carbon Dioxide in Water with the ωB97X by Yang[a,56]

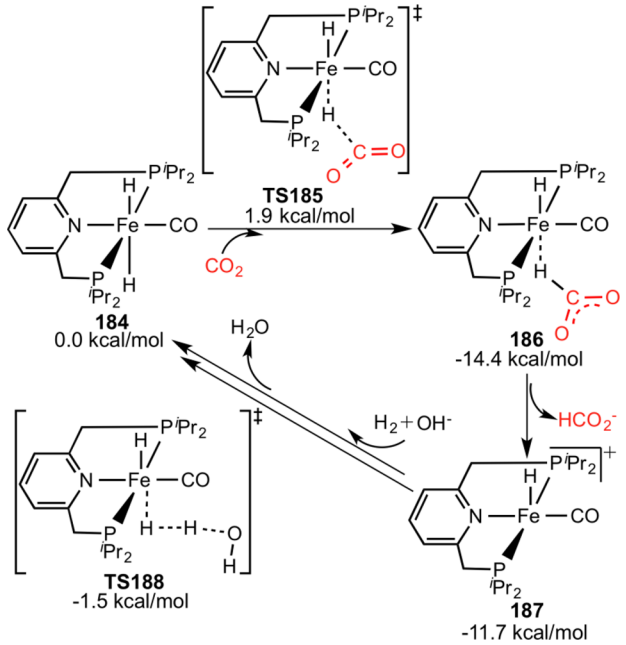

[a]Values are free energies.

Scheme 44. Proposed Mechanism for the Initial Dearomatization of 189 To Give 192 by Hofmann and Coworkers[57]

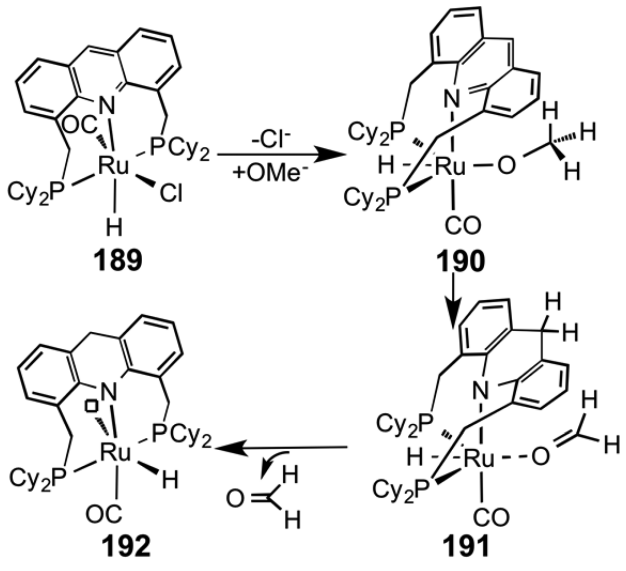

DOI: 10.1021/cs501875z
ACS Catal. 2015, 5, 1895−1913

catalytic cycle for alcohol amination with NH_3 is shown in Scheme 45. The active species **194** is generated from **193**, which

Scheme 45. Proposed Mechanism for the Amination of Alcohol with NH_3 by Hofmann and Coworkers[57]

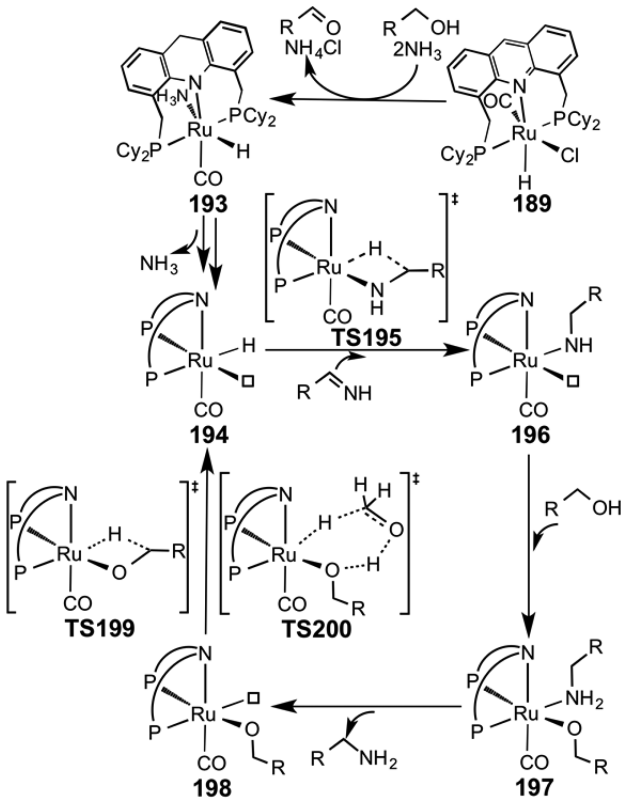

is formed from the precursor **189**. Complex **194** reduces the imine, which is formed by the condensation of the aldehyde with NH_3, via imine insertion into the Ru−H bond over transition state **TS195**, formation of intermediate **196**, protonation of the amino moiety by alcohol to form **197**, and dissociation of the primary amine product to generate complex **198**. The regeneration of **194** can occur either through inner-sphere β-hydride elimination transition state **TS199** or outer-sphere concerted hydrogen transfer transition state **TS200**. The calculations show that the most favorable pathway for this catalyst does not require metal−ligand cooperation.

4. CONCLUSION

In summary, we have reviewed theoretical studies on the mechanisms for the reactions mediated by transition metal complexes with noninnocent pincer ligands developed by Milstein and co-workers. These complexes represent a new mode of metal−ligand cooperation, which is proposed to involve an aromatization−dearomatization process of the pyridine or acridine-based PNP and PNN "pincer" ligands. The reported reactions are considered green chemistry and involve the unusual X−H (X = H, C, O, N, and B) activation processes and environmentally benign catalysis involving dehydrogenations and hydrogenations. The theoretical studies show that the aromatization−dearomatization process of the pyridine-based PNP and PNN "pincer" ligands plays important roles in providing the lowest energy pathway for some steps, whereas for other steps, the lowest energy pathways do not involve the aromatization−dearomatization process, even though it can be proposed as a reasonable pathway for some cases. For the reactions in which different mechanisms have been proposed, our recalculations on their rate-determining steps identified the most reasonable mechanism. In addition to the studies reported here, Milstein and co-workers continue to synthesize new types of compounds and report new transformations. Thus, theoretical studies will continue to be necessary to understand their mechanisms, and this Review will be helpful in pointing the directions needed to bring those theoretical studies to correct conclusions.

AUTHOR INFORMATION

Corresponding Author

*E-mail: haixia.li@chem.tamu.edu.

Notes

The authors declare no competing financial interest.

ACKNOWLEDGMENTS

The financial support from the National Science Foundation under CHE-1300787 is acknowledged. The computing resources of the Texas A&M Supercomputing Facility (http://sc.tamu.edu/) are also thanked here.

REFERENCES

(1) *Transition Metals for Organic Synthesis*; Beller, M., Bolm, C., Eds.; WILEY-VCH Verlag GmbH & Co. KGaA: Weinheim, 2004, Vol. *1*, pp 1−631.

(2) (a) Clapham, S. E.; Hadzovic, A.; Morris, R. H. *Coord. Chem. Rev.* **2004**, *248*, 2201−2237. (b) Ikariya, T.; Blacker, A. J. *Acc. Chem. Res.* **2007**, *40*, 1300−1308. (c) Grützmacher, H. *Angew. Chem., Int. Ed.* **2008**, *47*, 1814−1818. (d) Lyaskovskyy, V.; de Bruin, B. *ACS Catal.* **2012**, *2*, 270−279. (e) van der Vlugt, J. I. *Eur. J. Inorg. Chem.* **2012**, 363−375.

(3) (a) Milstein, D. *Top. Catal.* **2010**, *53*, 915−923. (b) Gunanathan, C.; Milstein, D. *Acc. Chem. Res.* **2011**, *44*, 588−602. (c) Gunanathan, C.; Milstein, D. *Science* **2013**, *341*, 1229712. (d) Gunanathan, C.; Milstein, D. *Chem. Rev.* **2014**, *114*, 12024−12087.

(4) (a) Reguillo, R.; Grellier, M.; Vautravers, N.; Vendier, L.; Sabo-Etienne, S. *J. Am. Chem. Soc.* **2010**, *132*, 7854−7855. (b) Song, C.; Qu, S.; Tao, Y.; Dang, Y.; Wang, Z.-X. *ACS. Catal.* **2014**, *4*, 2854−2865. (c) Friedrich, A.; Drees, M.; auf der Günne, J. S.; Schneider, S. *J. Am. Chem. Soc.* **2009**, *131*, 17552−17553. (d) Friedrich, A.; Drees, M.; Käss, M.; Herdtweck, E.; Schneider, S. *Inorg. Chem.* **2010**, *49*, 5482−5494. (e) Yang, X. *ACS. Catal.* **2013**, *3*, 2684−2688. (f) Yang, X. *ACS. Catal.* **2014**, *4*, 1129−1133.

(5) (a) Hehre, W. J.; Ditchfie, R.; Pople, J. A. *J. Chem. Phys.* **1972**, *56*, 2257−2261. (b) Francl, M. M.; Pietro, W. J.; Hehre, W. J.; Binkley, J. S.; Gordon, M. S.; Defrees, D. J.; Pople, J. A. *J. Chem. Phys.* **1982**, *77*, 3654−3665.

(6) Andrae, D.; Häussermann, U.; Dolg, M.; Stoll, H.; Preuss, H. *Theor. Chem. Acc.* **1990**, *77*, 123−141.

(7) Zhao, Y.; Truhlar, D. G. *J. Chem. Phys.* **2006**, *125*, 194101.

(8) Tao, J. M.; Perdew, J. P.; Staroverov, V. N.; Scuseria, G. E. *Phys. Rev. Lett.* **2003**, *91*, 146401.

(9) Grimme, S.; Antony, J.; Ehrlich, S.; Krieg, H. *J. Chem. Phys.* **2010**, *132*, 154104.

(10) (a) Lee, C. T.; Yang, W. T.; Parr, R. G. *Phys. Rev. B* **1988**, *37*, 785−789. (b) Miehlich, B.; Savin, A.; Stoll, H.; Preuss, H. *Chem. Phys. Lett.* **1989**, *157*, 200−206. (c) Becke, A. D. *J. Chem. Phys.* **1993**, *98*, 5648−5652.

(11) Zhao, Y.; Truhlar, D. G. *Theor. Chem. Acc.* **2008**, *120*, 215−241.

(12) (a) Chai, J.-D.; Head-Gordon, M. *Phys. Chem. Chem. Phys.* **2008**, *10*, 6615−6620.

(13) (a) McLean, A. D.; Chandler, G. S. *J. Chem. Phys.* **1980**, *72*, 5639−5648. (b) Krishnan, R.; Binkley, J. S.; Seeger, R.; Pople, J. A. *J. Chem. Phys.* **1980**, *72*, 650−654.

DOI: 10.1021/cs501875z
ACS Catal. 2015, 5, 1895−1913

(14) Clark, T.; Chandrasekhar, J.; Spitznagel, G. W.; Schleyer, P. v. R. *J. Comput. Chem.* **1983**, *4*, 294−301.
(15) Dunning, T. H. *J. Chem. Phys.* **1989**, *90*, 1007−1023.
(16) (a) Feller, D. *J. Comput. Chem.* **1996**, *17*, 1571−1586. (b) Schuchardt, K. L.; Didier, B. T.; Elsethagen, T.; Sun, L.; Gurumoorthi, V.; Chase, J.; Li, J.; Windus, T. L. *J. Chem. Inf. Model.* **2007**, *47*, 1045−1052.
(17) (a) Perdew, J. P.; Burke, K.; Ernzerhof, M. *Phys. Rev. Lett.* **1996**, *77*, 3865−3868. (b) Perdew, J. P.; Burke, K.; Ernzerhof, M. *Phys. Rev. Lett.* **1997**, *78*, 1396−1396.
(18) (a) Perdew, J. P.; Emzerhof, M.; Burke, K. *J. Chem. Phys.* **1996**, *105*, 9982−9985. (b) Adamo, C.; Barone, V. *J. Chem. Phys.* **1999**, *110*, 6158−6170.
(19) Peverati, R.; Truhlar, D. G. *J. Chem. Phys.* **2011**, *135*, 191102.
(20) Boese, A. D.; Martin, J. M. L. *J. Chem. Phys.* **2004**, *121*, 3405−3416.
(21) Yanai, T.; Tew, D. P.; Handy, N. C. *Chem. Phys. Lett.* **2004**, *393*, 51−57.
(22) Chai, J.-D.; Head-Gordon, M. *J. Chem. Phys.* **2008**, *128*, 084106.
(23) Peverati, R.; Truhlar, D. G. *Phys. Chem. Chem. Phys.* **2012**, *14*, 16187−16191.
(24) Henderson, T. M.; Izmaylov, A. F.; Scuseria, G. E.; Savin, A. *J. Chem. Theory Comput.* **2008**, *4*, 1254−1262.
(25) (a) Heyd, J.; Scuseria, G. E. *J. Chem. Phys.* **2004**, *121*, 1187−1192. (b) Heyd, J.; Scuseria, G. E. *J. Chem. Phys.* **2004**, *120*, 7274−7280.
(26) Vydrov, O. A.; Scuseria, G. E. *J. Chem. Phys.* **2006**, *125*, 234109.
(27) Purvis, G. D., III; Bartlett, R. J. *J. Chem. Phys.* **1982**, *76*, 1910−1918.
(28) Pople, J. A.; Head-Gordon, M.; Raghavachari, K. *J. Chem. Phys.* **1987**, *87*, 5968−5975.
(29) Fukui, K. *Acc. Chem. Res.* **1981**, *14*, 363−368.
(30) Marenich, A. V.; Cramer, C. J.; Truhlar, D. G. *J. Phys. Chem. B* **2009**, *113*, 6378−6396.
(31) Frisch, M. J.; Trucks, G. W.; Schlegel, H. B.; Scuseria, G. E.; Robb, M. A.; Cheeseman, J. R.; Scalmani, G.; Barone, V.; Mennucci, B.; Petersson, G. A.; Nakatsuji, H.; Caricato, M.; Li, X.; Hratchian, H. P.; Izmaylov, A. F.; Bloino, J.; Zheng, G.; Sonnenberg, J. L.; Hada, M.; Ehara, M.; Toyota, K.; Fukuda, R.; Hasegawa, J.; Ishida, M.; Nakajima, T.; Honda, Y.; Kitao, O.; Nakai, H.; Vreven, T.; Montgomery, J. A., Jr.; Peralta, J. E.; Ogliaro, F.; Bearpark, M.; Heyd, J. J.; Brothers, E.; Kudin, K. N.; Staroverov, V. N.; Kobayashi, R.; Normand, J.; Raghavachari, K.; Rendell, A.; Burant, J. C.; Iyengar, S. S.; Tomasi, J.; Cossi, M.; Rega, N.; Millam, J. M.; Klene, M.; Knox, J. E.; Cross, J. B.; Bakken, V.; Adamo, C.; Jaramillo, J.; Gomperts, R.; Stratmann, R. E.; Yazyev, O.; Austin, A. J.; Cammi, R.; Pomelli, C.; Ochterski, J. W.; Martin, R. L.; Morokuma, K.; Zakrzewski, V. G.; Voth, G. A.; Salvador, P.; Dannenberg, J. J.; Dapprich, S.; Daniels, A. D.; Farkas, O.; Foresman, J. B.; Ortiz, J. V.; Cioslowski, J.; Fox, D. J. *Gaussian 09, revision B.01*; Gaussian, Inc.: Wallingford CT, 2009.
(32) (a) Werner, H.-J.; Knowles, P. J.; Knizia, G.; Manby, F. R.; Schütz, M. *WIREs Comput. Mol. Sci.* **2012**, *2*, 242−253. (b) Werner, H.-J.; Knowles, P. J.; Knizia, G.; Manby, F. R.; Schütz, M.; Celani, P.; Korona, T.; Lindh, R.; Mitrushenkov, A.; Rauhut, G.; Shamasundar, K. R.; Adler, T. B.; Amos, R. D.; Bernhardsson, A.; Berning, A.; Cooper, D. L.; Deegan, M. J. O.; Dobbyn, A. J.; Eckert, F.; Goll, E.; Hampel, C.; Hesselmann, A.; Hetzer, G.; Hrenar, T.; Jansen, G.; Köppl, C.; Liu, Y.; Lloyd, A. W.; Mata, R. A.; May, A. J.; McNicholas, S. J.; Meyer, W.; Mura, M. E.; Nicklass, A.; O'Neill, D. P.; Palmieri, P.; Peng, D.; Pflüger, K.; Pitzer, R.; Reiher, M.; Shiozaki, T.; Stoll, H.; Stone, A. J.; Tarroni, R.; Thorsteinsson, T.; Wang, M. *MOLPRO, version 2012.1, a package of ab initio programs*; see http://www.molpro.net.
(33) Li, H.; Wang, Z. *Sci. Chin. Chem.* **2012**, *55*, 1991−2008.
(34) Zeng, G.; Guo, Y.; Li, S. *Inorg. Chem.* **2009**, *48*, 10257−10263.
(35) Iron, M. A.; Ben-Ari, E.; Cohen, R.; Milstein, D. *Dalton Trans.* **2009**, 9433−9439.
(36) Schwartsburd, L.; Iron, M. A.; Konstantinovski, L.; Diskin-Posner, Y.; Leitus, G.; Shimon, L. J. W.; Milstein, D. *Organometallics* **2010**, *29*, 3817−3827.
(37) Li, J.; Shiota, Y.; Yoshizawa, K. *J. Am. Chem. Soc.* **2009**, *131*, 13584−13585.
(38) Yang, X.; Hall, M. B. *J. Am. Chem. Soc.* **2010**, *132*, 120−130.
(39) Sandhya, K. S.; Suresh, C. H. *Organometallics* **2011**, *30*, 3888−3891.
(40) Khaskin, E.; Iron, M. A.; Shimon, L. J. W.; Zhang, J.; Milstein, D. *J. Am. Chem. Soc.* **2010**, *132*, 8542−8543.
(41) Anaby, A.; Butschke, B.; Ben-David, Y.; Shimon, L. J. W.; Leitus, G.; Feller, M.; Milstein, D. *Organometallics* **2014**, *33*, 3716−3726.
(42) Li, H.; Wang, X.; Huang, F.; Lu, G.; Jiang, J.; Wang, Z.-X. *Organometallics* **2011**, *30*, 5233−5247.
(43) Cho, D.; Ko, K. C.; Lee, J. Y. *Organometallics* **2013**, *32*, 4571−4576.
(44) Zeng, G.; Li, S. *Inorg. Chem.* **2011**, *50*, 10572−10580.
(45) Li, H.; Wang, X.; Wen, M.; Wang, Z.-X. *Eur. J. Inorg. Chem.* **2012**, 5011−5020.
(46) Sandhya, K. S.; Suresh, C. H. *Organometallics* **2013**, *32*, 2926−2933.
(47) Li, H.; Hall, M. B. *J. Am. Chem. Soc.* **2014**, *136*, 383−395.
(48) Qu, S.; Dang, Y.; Song, C.; Wen, M.; Huang, K.-W.; Wang, Z.-X. *J. Am. Chem. Soc.* **2014**, *136*, 4974−4991.
(49) Yang, X. *Inorg. Chem.* **2011**, *50*, 12836−12843.
(50) Cantillo, D. *Eur. J. Inorg. Chem.* **2011**, 3008−3013.
(51) Li, H.; Wen, M.; Wang, Z.-X. *Inorg. Chem.* **2012**, *51*, 5716−5727.
(52) Yang, X. *ACS Catal.* **2012**, *2*, 964−970.
(53) Hasanayn, F.; Baroudi, A.; Bengali, A. A.; Goldman, A. S. *Organometallics* **2013**, *32*, 6969−6985.
(54) Hasanayn, F.; Baroudi, A. *Organometallics* **2013**, *32*, 2493−2496.
(55) Hasanayn, F.; Harb, H. *Inorg. Chem.* **2014**, *53*, 8334−8349.
(56) Yang, X. *ACS Catal.* **2011**, *1*, 849−854.
(57) Ye, X.; Plessow, P. N.; Brinks, M. K.; Schelwies, M.; Schaub, T.; Rominger, F.; Paciello, R.; Limbach, M.; Hofmann, P. *J. Am. Chem. Soc.* **2014**, *136*, 5923−5929.
(58) Ben-Ari, E.; Leitus, G.; Shimon, L. J. W.; Milstein, D. *J. Am. Chem. Soc.* **2006**, *128*, 15390−15391.
(59) Kohl, S. W.; Weiner, L.; Schwartsburd, L.; Konstantinovski, L.; Shimon, L. J. W.; Ben-David, Y.; Iron, M. A.; Milstein, D. *Science* **2009**, *324*, 74−77.
(60) Chen, Y.; Fang, W.-H. *J. Phys. Chem. A* **2010**, *114*, 10334−10338.
(61) (a) Hermans, J.; Wang, L. *J. Am. Chem. Soc.* **1997**, *119*, 2707−2714. (b) Strajbl, M.; Sham, Y. Y.; Villa, J.; Chu, Z. T.; Warshel, A. *J. Phys. Chem. B* **2000**, *104*, 4578−4584.
(62) Gunanathan, C.; Ben-David, Y.; Milstein, D. *Science* **2007**, *317*, 790−792.
(63) Montag, M.; Zhang, J.; Milstein, D. *J. Am. Chem. Soc.* **2012**, *134*, 10325−10328.
(64) Zhang, J.; Leitus, G.; Ben-David, Y.; Milstein, D. *J. Am. Chem. Soc.* **2005**, *127*, 10840−10841.
(65) Gnanaprakasam, B.; Zhang, J.; Milstein, D. *Angew. Chem., Int. Ed.* **2010**, *49*, 1468−1471.
(66) Balaraman, E.; Khaskin, E.; Leitus, G.; Milstein, D. *Nat. Chem.* **2013**, *5*, 122−125.
(67) Srimani, D.; Ben-David, Y.; Milstein, D. *Angew. Chem., Int. Ed.* **2013**, *52*, 4012−4015.
(68) Langer, R.; Leitus, G.; Ben-David, Y.; Milstein, D. *Angew. Chem., Int. Ed.* **2011**, *50*, 2120−2124.
(69) Balaraman, E.; Gnanaprakasam, B.; Shimon, L. J. W.; Milstein, D. *J. Am. Chem. Soc.* **2010**, *132*, 16756−16758.
(70) Balaraman, E.; Gunanathan, C.; Zhang, J.; Shimon, L. J. W.; Milstein, D. *Nat. Chem.* **2011**, *3*, 609−614.
(71) Langer, R.; Diskin-Posner, Y.; Leitus, G.; Shimon, L. J. W.; Ben-David, Y.; Milstein, D. *Angew. Chem., Int. Ed.* **2011**, *50*, 9948−9952.
(72) Vogt, M.; Gargir, M.; Iron, M. A.; Diskin-Posner, Y.; Ben-David, Y.; Milstein, D. *Chem.—Eur. J.* **2012**, *18*, 9194−9197.
(73) (a) Gunanathan, C.; Milstein, D. *Angew. Chem., Int. Ed.* **2008**, *47*, 8661−8664. (b) Gunanathan, C.; Shimon, L. J. W.; Milstein, D. *J. Am. Chem. Soc.* **2009**, *131*, 3146−3147. (c) Gunanathan, C.; Gnanaprakasam, B.; Iron, M. A.; Shimon, L. J. W.; Milstein, D. *J. Am. Chem. Soc.* **2010**, *132*, 14763−14765.

DOI: 10.1021/cs501875z
ACS Catal. 2015, 5, 1895−1913